UNIVERSITY OF CAPE TOWN
IYUNIVESITHI YASEKAPA • UNIVERSITEIT VAN KAAPSTAD

Characteristics of Inertial Gravity Waves over Southern Africa as simulated with CAM-EULAG

by

David Ogier

Climate Systems Analysis Group

Environmental and Geographical Science

University of Cape Town

A thesis submitted to the Department of Environmental and Geographical Sciences University of Cape Town in fulfilment of the requirements for the degree of Master of Science (Atmospheric Science)

Supervisor: Babatunde J. Abiodun, University of Cape Town

PLAGIARISM DECLARATION

1. I know that plagiarism is wrong. Plagiarism is using another's work and to pretend that it is one's own.

2. I have used the Harvard as the convention for citation and referencing. Each significant contribution to, and quotation in, this thesis from the work, or works of other people has been attributed and has been cited and referenced.

3. This thesis is my own work.

4. I have not allowed, and will not allow, anyone to copy my work with the intention of passing it off as his or her own work.

5. I acknowledge that copying someone else's assignment or essay, or part of it, is wrong, and declare that this is my own work.

SIGNATURE: Signed by candidate DATE: 2013/05/20

Signature Removed

To whom it may concern,

I (Keith Williams) hereby confirm that I have edited David Ogier's dissertation entitled: "Characteristics of Inertial Gravity Waves over Southern Africa as simulated with CAM-EULAG".

I am the holderof an MA in English Language and Literature from UCT and have more than 17 years' experience in editing Parliamentary documents and academic theses.

Keith Williams

Abstract

Inertial gravity waves are ubiquitous in the atmosphere and play an important role in circulation, momentum and mixing in the atmosphere; yet there is a dearth of studies on the characteristics of inertial gravity wave activity over Southern Africa. This thesis presents a compressive analysis and discussions on characteristics of inertial gravity waves over the topographically and climatologically complex region of Southern Africa. It uses simulation data from a global model with grid-stretching capability. The horizontal variance analysis for vertical wind is used to identify three zones of strong wave activity as: southern Namibia (MWZ1), to the east of the Drakensberg (MWZ2) and over the Cape Fold Belt (MWZ3). MWZ1 and MWZ2 show seasonal persistence of wave activity, while MWZ3 exhibits activity only during the winter and spring seasons.

Self-Organising Maps provide a robust account of the horizontal distribution of wave activity in the lower troposphere, while the vertical cross-section, which illustrates the vertical structure of the wave and associated zonal wind, further confirms the causes of vertical motion to be convective activity and orographic influence. The strength of the wave activity is related to the speed and orientation of the horizontal wind. The maximum wave activity occurs in winter (MWZ2) and spring (MWZ1). Results of spectral analysis show that inertial gravity wave activity in MWZ1 is influenced by both convection and orography, while the wave activity in MWZ2 is primarily due to horizontal wind rising over the Drakensberg Range and propagating to the east.

Acknowledgements

This work has resulted from the dedicated assistance of many special and unique individuals and research groups. I am grateful to so many people that have helped me conclude this work. Only a few of the most influential people are listed below.

My supervisor, Dr Babatunde J. Abiodun, who has constantly inspired me to do more and challenged my understanding and approach. Thank you for all your hard work, unending patience and desire for excellence above anything I could have asked.

Special thanks also go to the following:

Dr Joseph M. Prusa, who has provided technical support and shared understanding of wave development and propagation.

Prof. Bruce Hewitson who has provided insight on academic writing style and inspiration.

Penny Driver who has been unwavering friend, full of support and assistance both technically and emotionally beyond what could be expected or deserved in especially difficult circumstances.

Shazza Bowen-Davies who has giving up so much time doing the final proofing; for support and friendship.

Rory Grandin and Hayley McIntosh for the friendship, support and consistent selfless technical assistance.

Members of the Climate Systems Analysis Group (CSAG) for the extra assistance and technical advice.

To the Centre for Scientific and Industrial Research (CSIR) for the use of the Centre for High Performance Computing (CHPC) resources.

To University of Cape Town (UCT) for the academic support and use of the university facilities.

I also wish to acknowledge the use of NOAA's Pacific Marine Environmental Laboratory Ferret program for analysis and graphics presented in this work.

Lastly I would like to thank Penny-Jane Cooke for being my everything.

Table of Contents

List of Figures:

Chapter 1. Introduction

An atmospheric wave is a periodic oscillation (or disturbance) in the atmosphere. The signature of atmospheric waves can be seen in the fields of atmospheric variables such as temperature, wind-velocity pressure and geo-potential height. The waves may either propagate with time (travelling waves), or remain stationary (standing waves). Atmospheric waves have various spatial and temporal scales, ranging from small-scale (like gravity waves) to large-scale planetary waves (like Rossby waves). They are the result of restoring forces acting as a disturbance to standard flow in the atmosphere (Prusa et al., 1999).

Although any mechanism can initiate atmospheric waves, a violation of the quasi-geostrophic balance (between pressure and wind fields) in the atmosphere usually initiates wave activity (Gavrilov and Fukao, 2001). For the purposes of this work, wave activity is defined as a noticeable oscillatory deviation from the standard atmosphere, as shown by various statistical methodologies performed on the vertical wind field. Further methodological specific definitions of wave activity are presented.

1.1 Importance of atmospheric waves

Wave activity can be found anywhere in the atmosphere, and the activity influences atmospheric motions at all scales. On local and synoptic scales, waves enhance atmospheric mixing and transport energy and momentum from the region of their excitation towards the middle and upper atmosphere (Baumgaertner and Mcdonald, 2007). On the meso-scale, in addition to the above, atmospheric waves can produce thermal variations and induce condensation and precipitation in isolated cloud bands (Geller et al., 2006).

On a global scale, the transport and deposition of momentum by waves are important in explaining global atmospheric circulation (Plougonven et al., 2003). Planetary scale waves traverse the globe and affect weather from sub-daily to seasonal time scales. The coupling between wave dynamics and moisture makes the atmospheric motions more complex in the tropics than in mid-latitude, because large-scale waves in the tropics can cause tropical convection, which later feeds back into the circulation through the release of latent heat in

storms. Hence, wave activity plays substantial roles in the atmosphere and a better understanding of the activity can enable more skilful weather forecasting.

Most previous studies on inertial gravity waves focused on the northern hemisphere (i.e. Nicolls et al., 2010, Chang et al., 2011, Shutts and Vosper, 2011), or on the Andes range (Vosper, 2010) as an excitation source. Identification of wave activity is problematic owing to its inconsistent nature and the resolutions required in capturing it, and therefore the limited observational network, particularly in Southern Africa, reduces the potential for wave study in the region (Hemer et al., 2010; Allen and Vincent, 1995). Additionally, the study of vertically oscillating waves has long been secondary to horizontal atmospheric dynamics. However, the advancements in computing are allowing simulation of the global atmosphere at higher resolutions and thereby reducing the need for wave parameterization (Hardiman et al. (2010). Moreover, this has been done by Sato et al. (2009) to study the dominant sources and propagation of gravity waves in the mesosphere with a horizontal resolution of 60km. Yet as Fritts and Alexander (2003) states, gravity wave horizontal scales vary between 15 and 300 km with periods of 20 – 100 minutes. This work therefore simulates the global atmosphere in CAM-Eulag (CEU), a non-hydrostatic global climate model with an adaptive grid resolution of approximately 10 km over Southern Africa and up to 150 km over the rest of the globe (Figure 3.1).

1.2 Types of atmospheric waves

The characteristics of atmospheric waves are influenced by various factors such as location, seasonality, local and larger-scale excitation mechanisms, as well as atmospheric conditions (Fritts and Alexander, 2003). However, the meteorologically relevant waves in the atmosphere are pure gravity waves, inertia waves and Rossby waves, inertia gravity waves, and easterly waves (Fritts and Alexander, 2003).

Pure gravity waves are sinusoidal disturbances that propagate vertically and horizontally in the atmosphere away from a region of excitation (Nappo, 2002). Gravity waves can be initiated by thermal convective activity, orographic upward motion, frontogenesis and oscillations of jet streams (Prusa et al., 1999; Plougonven and Snyder, 2005). They are normally present in the meso-scale and have periods that vary from tens of minutes to a few

hours, and wavelengths that vary from 15km to 300km (Fritts and Alexander, 2003; Kuester et al. 2008).

Conversely, larger-scale inertia waves are driven by the planetary scale geostrophic balance (pressure gradient and Coriolis force; Vanneste, 2013). Rossby waves, which have periods of several hours to several days, influence the daily weather in the mid-latitudes and subtropics (Beguin et al., 2012; Vanneste, 2013), whilst inertia waves account for a significant part of the large-scale variability in the tropics (Zagar et al., 2009). Although they are horizontally oscillating waves, inertia waves can also contribute to vertical wind activity, as geostrophic winds and horizontal wind in Rossby waves interact with (and rise over) orographic or convective barriers (Ellrod, 1991; Fritts and Alexander, 2003). Moreover, if the balance of atmospheric forces is not perfect, these waves may present a vertical component through variations in the hydrostatic buoyancy balance (Vanneste, 2013), forming inertia gravity waves.

Inertia gravity waves, which are predominantly excited by orography or convection (Vanneste 2013), are inherently active in both vertical and horizontal directions. These waves are more important for atmospheric mixing than momentum transport, as in the case of gravity waves (O'Sullivan and Dunkerton, 1995). An example of the formation of inertia waves occurs when westerly flows encounter the Andes range and results in cyclogenic inertia gravity waves with a large wavelength, featuring frequencies close to the Coriolis frequency (Plougonven et al., 2003; Llamedo et al., 2009). These longer waves are influenced by the earth's rotation and are deflected horizontally; hence they oscillate both vertically (like gravity waves) and horizontally (like inertia waves). Like pure gravity waves, inertia gravity wave generation, intensity, propagation and dissipation are altered by seasonal variations of background wind and temperature (Gavrilov and Fukao, 2001). The inertial wave activity can only be understood when the characteristics are studied relative to their seasonal and geographical variability, and with a particular focus on sources (Zhang et al., 2010).

The last wave of focus is the African easterly wave, which consists of large-scale horizontal oscillations in the troposphere over tropical central Africa and has periods of approximately

4 days and wavelengths of about 3000 km (Burpee, 1972; Bain et al., 2011). Their excitation has been a contentious issue, but there is a general consensus that waves are generated through a strong relationship between African topography and upstream convective triggers (Ventrice and Thorncroft, 2012). They act as transporters of heat and moisture from the Indian Ocean and subsequently have a large influence on West African rainfall in particular. Moreover, they are initial forerunners of tropical storm and cyclone activity over the tropical Atlantic (Ventrice and Thorncroft, 2012). Additionally, Ratna et al. (2012) presents a strong link between strong convective activity in Namibia and Botswana associated with easterly waves and the development of the tropical temperate trough system which, in turn, is influential in the spring or early summer climate of Southern Africa.

1.3 Climate of Southern Africa

The climatology of Southern Africa is described in Tyson and Preston-Whyte (2002), Dube (2002) and Crétat et al. (2011). The climate of Southern Africa is influenced by its relative position amidst the major atmospheric dynamics of the southern Hemisphere, both tropical and mid-latitude (Dube, 2002; Crétat et al., 2011). The rainy season peaks in late austral spring to summer linked to the southern limb of the Inter-Tropical Convergence Zone (ITCZ) (Crétat et al., 2011) and tropical-temperate trough interactions (Todd et al. 2004). During the remainder of the year semi-arid conditions persist.

Located between the latitudes of 20^{o}S and 36^{o}S, Southern Africa is subject to a wide variety of wave activity, such as the mid-latitude frontal systems in winter, convective tropical easterly waves and the tropical temperate trough in spring and early summer (Dube, 2002). Southern Africa is characterized by general convection in the warmer months and experiences year-round variability in orographic wave excitement based on seasonal horizontal winds (Tyson and Preston-Whyte, 2002). Cut-off low systems peak in the transition seasons of autumn (March – May, MAM) and spring (September – November, SON), and contribute to the variability of horizontal wind (Mason and Jury, 1997). During austral winter (June – August, JJA) horizontal winds, forced by frontal migration, tend to be westerly in the southern part of the country and north-westerly over the interior. Continental high pressure systems are often present in winter. Winds are weaker during the summer months (December – February, DJF) owing to decreased geostrophic potential and

often exhibit continental low pressures as convective activity peaks during the day (Mason and Jury, 1997).

Southern Africa, situated on a continental craton, features mountain ranges that influence orographic uplift of air (Moore, 2009; Janney et al., 2010). As shown in Figure 1.1, these mountains form a horseshoe-shaped escarpment around an inland plateau (Moore, 2009). The escarpment features the meridionally oriented Groot Karas Mountains (in south Namibia), the zonally oriented Cape Fold Belt (in Western and Eastern Cape, South Africa), and the Drakensberg range that curves from a zonal to a meridional orientation (in Kwa-Zulu Natal, South Africa). Because the meridionally oriented ranges are orthogonal to the zonally dominated horizontal winds (particularly in winter), they will excite more wave activity than the zonally oriented ranges. The topography on the eastern parts of Southern Africa can also trigger meso-scale convective systems (Crétat et al., 2011). Southern Africa is bordered by ocean on three sides, meaning that there is minimal short-wave activity entering the region from other sources and gravity wave activity presented will likely have its origin in Southern Africa. However, the warm east coast and cold west coast currents enhance the thermal gradient over Southern Africa (Crétat et al., 2011).

1.4 Aim and objectives

The aim of the present work is to study the characteristics of simulated inertial gravity waves over Southern Africa, focusing on the geographical and seasonal variations of the waves. The simulation is performed with a non-hydrostatic global climate model (CAM-EULAG) with high resolution over Southern Africa. The objectives of the study are to:

- evaluate the capability of CAM-EULAG in simulating global and regional climate features over Southern Africa;
- identify the hot spots or sources of inertial gravity waves over Southern Africa;
- study the characteristics (i.e. horizontal and vertical structure, and energy spectrum) of the inertial gravity wave over the region; and
- examine how these characteristics of the inertial waves vary with seasons.

The thesis is divided into five chapters. The literature review in Chapter 2 details how the understanding of atmospheric waves has evolved with time and the various approaches that

have been adopted in previous studies to study the waves. It also presents an indication of the advantages and disadvantages of the approaches. The chapter also reviews the challenges that the previous studies faced in studying inertial gravity waves over Southern Africa. Chapter 3 presents the methodology of the thesis; it describes CAM-EULAG and the simulation set-up used in the study, and describes the statistical approaches used in analyzing the simulations data. Chapter 4 presents and discusses the results of the model validation, while Chapter 5 presents and discusses the characteristics of the simulated inertial gravity waves over Southern Africa. Chapter 6 gives the concluding remarks, considers the limitations of the study, and makes suggestions for future studies.

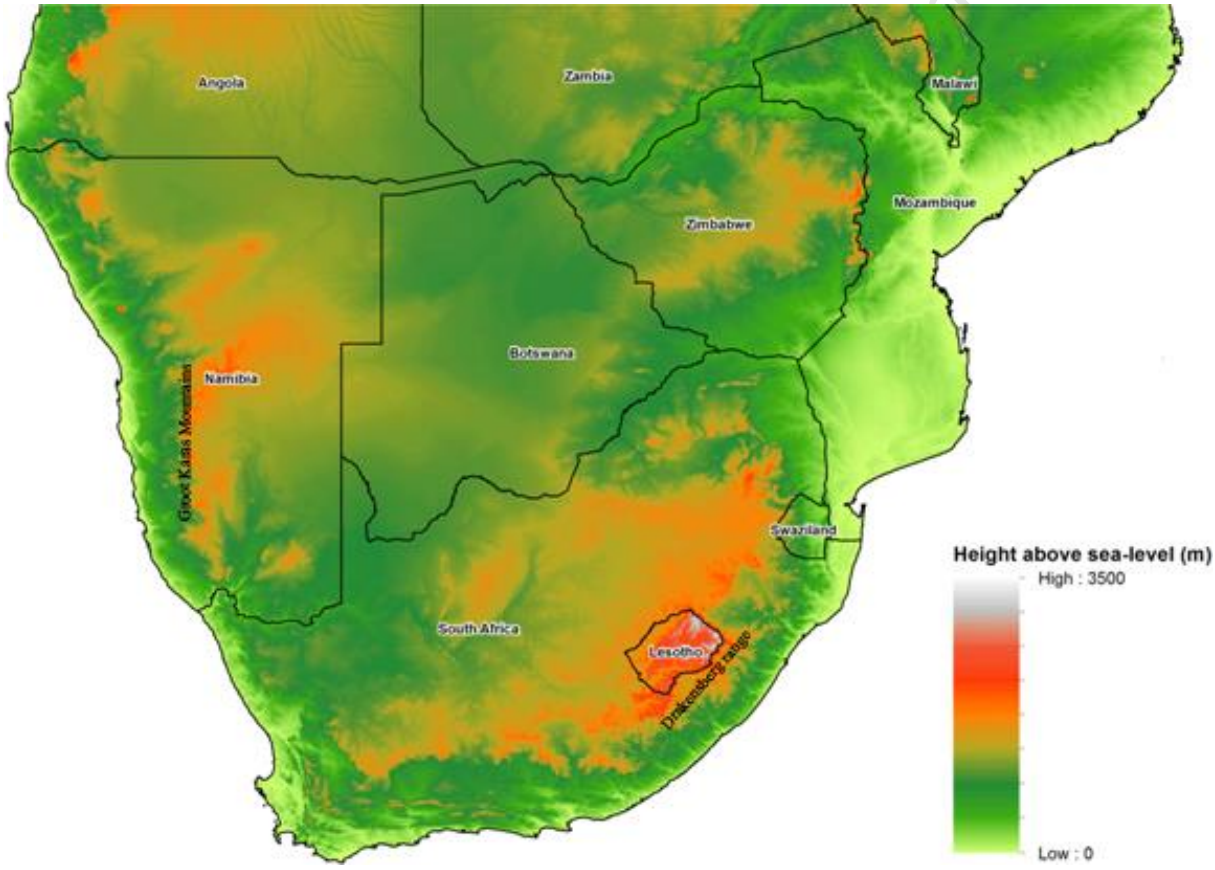

Figure 1.1: Shuttle Radar Topography Mission elevation data of the Southern African Domain

Chapter 2. Literature Review

This chapter reviews previous studies on atmospheric waves, focusing on how the understanding of atmospheric waves has evolved over time, and on the different approaches of the studies in detecting and studying the waves. It also reviews the few studies available on inertial gravity waves over South Africa.

2.1 History of atmospheric wave studies

2.1.1 Inertia Waves

Hardiman et al. (2010) provides a review on wave studies and emphasises the importance of early studies in building knowledge on wave generation, propagation, energy and mixing. Atmospheric wave study was pioneered by Rossby et al. (1938) and Rossby (1940); these authors studied the characteristics, propagation and impacts of large-scale waves. Rossby et al. (1938) showed that the influence of wave activity is present in every aspect of the atmosphere. Large-scale horizontal waves induce mixing and vertical shear stress within the wave system, as well as further influencing the free atmosphere outside the wave system. Rossby (1940) stated that the wave activity is responsible for many of the seasonal climate patterns and day-to-day weather variations, and showed that vorticity is more important than gradient wind in determining the characteristics of inertia waves in a mid-latitude jet stream.

However, Hardiman et al. (2010) argued that, while those early studies on inertia wave are important in building knowledge on wave generation, propagation, energy and mixing; they lacked information on broader scale wave interactions and influences because of the scarcity of observational data and computational power available during the studies. Using the understanding that westerly jet activity influences the pattern of wave propagation as suggested by barotropic Rossby-wave theory, Ambrizzi and Hoskins (1997) simulated Rossby wave propagation in a baroclinic atmosphere. They found that the domination of the wave progression by westerlies is in line with barotropic models simulation and observation. Domeisen and Plumb (2012) studied the interactions between inertia waves and tropospheric synoptic scale waves. In their study, while modelling the southern hemisphere with the view of assessing Stratospheric Sudden Warmings, they truncated the simulation to

allow only zonal waves (number 1 or 2), thus filtering out the synoptic influence. The results showed an increase in the strength of the long-wave activity and subsequently more active stratospheric warming events. Their conclusion was that Rossby wave baroclinic instability is suppressed by troposphere synoptic waves.

Freitas and Rao (2011) studied changes in characteristics and propagation associated with stationary Rossby waves under the influence of regional climate change with NCEP-NCAR reanalysis data in the periods 1948 – 1978 and 1979 – 2000. Their results showed a tendency for stationary Rossby waves to occur in the northern hemisphere's North Atlantic subtropical jet region and Asian jet stream. They further discovered that fluctuations of tropical SST favoured stationary waves in the polar jet, in the southern hemisphere, and that during stronger El Niño events stationary wave tendency is reduced in the northern hemisphere, but increased in the southern hemisphere (i.e. in the Australian and polar waves).

2.1.2 Gravity Waves

The influence of gravity waves on the atmosphere was first identified by Hines (1960), who attributed irregular motions in observational soundings in the ionosphere to gravity wave activity. Building on this, Hodges (1967) and Hines (1971) showed that gravity waves are important in transporting horizontal momentum generated in the troposphere to the middle and upper atmosphere. Focusing on wave saturation processes at the small and meso-scales, these authors developed a linear theory for parameterizing gravity wave effects on the interchange of energy by air parcels. Mied (1976) showed that even a gravity wave with infinitesimal amplitude can grow in amplitude and extract energy from bigger internal gravity waves. Yuan and Fritts (1989) combine the linear and non-linear theories to study the influence of mean vertical shear induced by large amplitude waves on the atmosphere, and concluded that the presence of gravity wave activity supports a wide range of dynamical instabilities with large growth rates.

Bretherton (1966) studied gravity wave propagation from the troposphere to upper atmosphere and found that if a wave group has the same velocity as the internal gravity waves, the frequency and horizontal components of the wave number are constant. He theorized that if a wave train of this type encounters a critical vertical level with a mean

wind that has a greater speed than the wave speed, the wave cannot propagate through that level; hence, the wave energy is reflected or ducted. Monserrat and Thorpe (1996) used Bretherton's (1966) theory to explain the observation of a long-lived, energy-retaining gravity wave that was ducted by a critical shear layer of stronger wind. It was the ducting of the wave train that enhanced the longevity and energy retention of the internal gravity wave.

Lindzen (1981) studied gravity wave breaking, and the associated turbulence, using atmospheric momentum measured from rocket launches. He examined turbulence generation by small amplitude waves and by the mean winds, and suggested that gravity wave breaking occurs at a greater altitude in summer than in winter (70km and 50km, respectively). In addition, he suggested that turbulence generated by gravity wave breaking is subject to a form of ducting presented by Bretherton's(1966) work, because critical vertical levels hinder the upward propagation of this disturbance.

Since gravity waves are fundamental to atmospheric circulation, some studies have investigated how to include the influence of gravity waves in GCM simulations through parameterization. Richter et al. (2010) studied the gravity wave parameterization schemes of orographic, frontal and convectively generated waves in the Whole Atmosphere Community Climate Model (WACC) and showed that parameterization schemes can have significant influence when simulating the middle and upper atmospheric features. Hence, there is need for more studies to fine tune parameterization schemes for a better simulation of the atmosphere; however, models with high resolutions do not need gravity parameterization.

2.1.3 Inertia Gravity waves

Cahn (1945) studied the momentum and energy relationships of waves. Using mathematical analysis, he proved that, in a fluid medium with a degree of curvature, momentum change in a localized zone results in a vertically propagating oscillation in that medium. This can be expressed as cyclical horizontal wind interacting with a large-scale orographic barrier and induces the excitation of an inertia gravity wave (Geisler and Dickinson, 1972). Charney and Drazin (1961) studied vertical propagation of inertia gravity waves in the atmosphere, and gave a hypothesis that large-scale inertia gravity wave motions do not penetrate above the

middle stratosphere and are rather reflected in the presence of easterly wind or a westerly wind above a maximum threshold in the mid-latitudes. This hypothesis, however, was refuted by Newell and Dickinson (1967), who observed the occurrence of these inertia waves in the middle and upper atmosphere under these conditions.

Further inertial gravity waves studies focused on the influence of inertial gravity waves on species mixing and momentum transport. Newell (1964) studied the influence of inertia gravity waves on trace substances, and found that the variance of ozone and radioactive tracers peaked in the vicinity of inertia gravity waves and jet streams, while minimal variance was observed in areas exhibiting a mean stratified atmosphere. He concluded that wave activity alters ozone and radioactive trace substance transport. Wallace and Newell (1966) also studied the influence of inertial gravity wave activity. Focusing on eddy fluxes, they examined the effect of inertia gravity waves' intensity on zonal wind in the low and middle latitude stratosphere, and concluded that variability in wave strength is sufficient to account for the biennial oscillation of westerly wind in the low latitudes.

Fritts and Rastogi (1985) reviewed the theory of gravity wave mixing and turbulence in the presence of convective and dynamical instability, and compared the theory to observational evidence from the middle atmosphere. They concluded that convectively generated inertia gravity waves primarily influence momentum transport through large vertical wavelengths, whilst Kelvin-Helmholtz dynamic instability, which occurs in the presence of vertical shear, has more influence than gravity waves on species mixing. The findings were contradicted by O'Sullivan and Dunkerton's (1995) study on the generation of inertia gravity waves in baroclinic instability. O'Sullivan and Dunkerton (1995) found that while the consequence of momentum transport is of great significance to atmospheric circulation, species constituent mixing of ozone, trace gases, moisture and heat is even more so. However, the measure of significance is subjective, based on the regions and approaches of each study. Both influences of inertia gravity waves are important and have subsequently been studied in-depth.

2.2 Detection of Atmospheric Waves

The diversity in excitation and subsequent nature of atmospheric waves calls for different methodologies in capturing the signature or influence of these waves. The waves can be studied theoretically, observationally, or with model simulation (Fritts and Alexander, 2003). The literature presented here focuses on detecting wave activity using remote sensing tools (such as synthetic aperture radar or infrared sounding from satellite images), *in situ* instruments (like ground-based radar and radiosondes), and atmospheric model simulations.

2.2.1 Remote sensing approach

From an observational perspective, remote sensing plays a key role in wave detection. Magalhaes et al. (2011) used ERSSAR and ENVISAT synthetic aperture radar imagery to detect wave-like signatures in the Red Sea area. They were able to characterize perturbations in the imagery as gravity waves, based on the calculated phase speed using weakly nonlinear wave theory and wavelengths, which have a peak occurrence between April and September. Large-scale wave analysis was undertaken by Pancheva and Laštovička (1998) using the satellite-based CRISTA 1 limb-scanning data to study 7-day planetary waves in the lower ionosphere. They found wave activity peaks at the 3-5, 6-8, and 15-23 day periods. This study was followed up by Clark et al. (2002) who used the High Resolution Doppler Imager on board the Upper Atmospheric Research Satellite to study latitudinal structure and seasonal variations of planetary scale waves. They found evidence of planetary waves with a long period (2–20 days) that change frequency smoothly over time in the lower thermosphere.

Eckermann and Wu (2012) used atmospheric infrared sounder imagery to capture long-wavelength gravity waves' temperature perturbations in the atmosphere, and found that wave activity was considerably stronger in austral winter between 40°S - 70°S with additional localized orographic wave activity around the Andes, New Zealand Alps and Antarctic. However, the remote sensing failed to detect similar wave activity in 24°S - 40°S despite the significant topography in Southern Africa and Australia. The study detected the wave activity by reducing background imagery noise levels and filtering out only the wave radiance. However, the authors admitted that the wave detection was problematic, because the orographic waves are near the resolution limits of nadir and limb-capture radiances. The

problem confirmed Baumgaertner and Mcdonald's (2007) statement that direct observation of wave activity using remote sensing is difficult or often impossible, and that wave detection can be done through variables such as vertical wind or potential temperature which are easier to measure. Alternatively, model simulation provides the full dataset of atmospheric variables. This was also echoed by Magalhaes et al. (2011), who observed that the difference between ocean and atmosphere wave signatures was problematic and might lead to misclassification. In addition, even though spatial coverage and duration from satellite imagery are extensive, from a purely logistical point of view, multiple satellite images are needed to estimate some characteristics of waves. As Magalhaes et al. (2011) observed, the daily image record often does not have the sufficient temporal resolution or the needed sunlight to present detailed wave analysis. Hence, satellite data fails to detect all multi-variable dynamics in high resolution (Magalhaes et al., 2011).

2.2.2 In situ measurement methods

Several studies (i.e. Allen and Vincent, 1995; Wang and Geller, 2003; and Wang et al., 2005) have used analysis of multi-station radiosonde observations to study atmospheric waves. Allen and Vincent (1995) analyzed a single year of data from 18 stations in Australia and Antarctica and concluded that wave activity peaked during the wet winter season. Wang and Geller (2003) utilized five years' data from 94 stations in the US. They found that background horizontal wind speeds determines the intrinsic frequency of gravity waves, gravity wave activity peaks in winter, and the dominating horizontal wavelength decreases with increasing latitude. Wang et al. (2005) expanded the earlier study of Wang and Geller (2003) by using radiosonde stations in a larger geographical area, but found similar results as in Wang and Geller (2003). In the study, the peak of gravity wave activity was in winter and there was a persistent strong orographic gravity wave over the Rocky Mountains.

However, a multi-station radiosonde observation network is usually too sparse for climatological analysis. To overcome this shortfall, Zhang et al. (2010) extended the datasets of Wang and Geller (2003) and Wang et al. (2005) and studied the seasonal and latitudinal variations of wave energy density over a wide geographic region, but this can only be achieved where adequate datasets exist. The findings of Zhang et al. (2010) were similar to those of the previous studies, although they found that gravity wave activity was stronger in

the troposphere than in the stratosphere at the lower latitudes and suggested that this may be due to a strong gravity wave source in the tropopause.

The use of ground-based radar instruments can provide continuity of high resolution, but only local data. Hocking and Kumar (2011) used two radar arrays with a combined 18-year dataset to study quasi-7-day planetary waves in the polar Mesosphere and Lower Thermosphere (MLT). The receiver antennas were calibrated to the required phase to capture planetary scale waves. However, this resulted in the filtering out of all other atmospheric waves, which prevented the study from presenting holistic climatological data. Nicolls et al. (2010) presented a short-term study of observed inertia gravity waves captured by the Poker Flat Incoherent Scatter Radar. They used the data to advance understanding of inertia gravity wave generation by jet streams in the troposphere and regions of significant geostrophic adjustment. They suggested that inertial gravity waves noted in the observation over Alaska was generated and propagated from northern Russia. This same instrument was utilized previously to capture three-dimensional measurements and infer wave propagation directions, periods, and horizontal wavelengths of upper ionosphere gravity waves' dynamics (Nicolls and Heinselman, 2007). Jayaraman et al. (2010) argued that these short-term studies with limited observational capacity do not provide sufficient data for climatological analysis. Jayaraman et al. (2010) therefore presented radar observation undertaken with the Study of Atmospheric Forcing and Responses (SAFAR). Previous radar campaigns were done in isolation, with little collaboration; therefore those studies presented data for only parts of the atmospheric spectrum and only at particular vertical levels with varying timeframes. SAFAR, on the other hand, was a comprehensive five-year study of the entire atmospheric column over Gadanki (India), using 18 localized instruments with varying temporal resolution, Doppler Weather Radar data – sourced from Chennai (India Met Dept.) and satellite observations (Jayaraman et al., 2010). Mesosphere-Stratosphere-Troposphere (MST) radar and Lidar were the core instruments for the study, but all the instruments complemented one another to provide coverage from surface layer to the ionosphere. Hence, SAFAR provided an integrated dataset for studying the vertical coupling between natural and anthropogenic forcing for the whole vertical column (Jayaraman et al., 2010). However, despite the exorbitant cost of the campaign, the results are regional.

2.2.3 Atmospheric model simulations approaches

The use of model or observational reanalysis data for studying atmospheric waves is not constrained by resolution (as with the satellite approach) or limited by the regional and duration limitations (as with the *in situ* measurement approach). The modelling approach is able to provide a three-dimensional dataset of sufficient spatial and temporal resolution to resolve most scales of atmospheric waves (Zagar et al., 2009). The main shortcoming when using the modelling approach is the lack of direct observations of wind profiles and other atmospheric variables to aid the model simulations (reanalysis). Zagar et al. (2009) reduced this uncertainty by comparing energy spectra from reanalysis datasets to Data Assimilation Research Test bed – Community Atmospheric Model, European Centre for Medium-Range Weather Forecasts and National Centres for Environmental Prediction data. They found that the results of the reanalysis data were consistent with the linear theory of vertically propagating equatorial waves.

Grimsdell et al. (2010) applied the modelling approach to study convectively generated waves. In the study, a three-dimensional, non-linear, non-hydrostatic, cloud-resolving model is forced, with observed scanning radar with varying heating field data to simulate the atmosphere responsible for generating gravity wave activity. The model output was validated against satellite imagery from the Atmospheric Infrared Sounder. Grimsdell et al. (2010) concluded that model data agreed well with wave patterns observed by remote sensed imagery and that this method could prove useful for evaluating and improving global model gravity wave parameterizations. They suggested that the output could be confidently analysed for excitation activity.

Another study that examined wave resolution in global models (MetUM) was Hardiman et al. (2010). The study looked at climatologies of ensemble runs focusing on stationary waves, seasonal means and annual cycles at moderate (2.58 latitude x 3.758 longitude) and high (1.258 latitude x 1.8758 longitude) resolutions. The results showed that the model datasets had good agreement with the reanalysis data. Beguin et al. (2012) argued that simulated synoptic scale features should be compared against observation to fully validate a climate model. To that end, they used ECHAM5-HAM to simulate a synoptic scale breaking Rossby

wave and validated the frequency and location of the occurrence feature. Ensemble 44-year simulations with differing vertical and horizontal resolution regular grids were validated against ERA-40 reanalysis data and showed varied results. All the simulations underestimated large Rossby wave breaking events, but the bias decreased with increase in the resolution model. In contrast, the high resolution simulations overestimated the occurrence of the smaller Rossby wave breaking.

Ndarana and Waugh (2010) used a 30-year meteorological reanalysis dataset to create the climatology of breaking Rossby waves in the southern hemisphere. The objectives of the work were twofold, firstly to study the morphology and occurrence of breaking Rossby waves in each of their four states (cyclonic or anti-cyclonic curvature and polar- or equator-ward wave activity flux); and secondly to present the spatial and temporal changes of the Rossby wave and the relationship with the tropospheric jets. They concluded that anti-cyclonic breaking is more common than cyclonic breaking, and wave breaking activity moves to high latitudes in winter and to lower latitudes in summer. In addition, the authors found significant seasonal changes in Rossby wave breaking resulting from movement of the tropospheric jet and the characteristics of the tropopause.

Chandran et al. (2011) used the Atmosphere Community Climate Model to determine the influence of gravity waves on thermal mixing in the presence of stratospheric sudden warming. The model, incorporating troposphere and stratosphere observational data, resolved the propagation of planetary Rossby waves, and simulated the interaction of waves with zonal mean flow that causes these warming events. The study was able to simulate the sudden stratospheric warming and determined that this event hinders penetration of eastward propagating gravity waves into the mesosphere. After the warming event, gravity wave activity returned to normal.

Nevertheless, all these modelling studies used either the global climate model or the regional climate model nested with a global model in studying the atmospheric waves. While GCMs simulate the entire globe with sufficient resolution to resolve synoptic circulations well, smaller-scale mesoscale features that require a higher resolution are parameterised (Richter et al., 2010). Parameterisations can lead to simulation inaccuracy (Song and Chun,

2006 and Zhang, 2010). Using the global atmosphere at sufficiently high resolution to resolve mesoscale wave activity is computationally very expensive. Alternatively, RCMs have adequate resolution to simulate mesoscale features which cover a limited area, but they require GCM or reanalysis data to force external dynamics. This forcing may produce boundary condition errors, which can propagate into the model domain and contaminate the simulated mesoscale features.

The shortcomings of both GCMs and RCMs are overcome by the use of a Stretched Grid Global Climate Model (SGGCM).A SGGCM is a GCM that uses an adaptive grid algorithm to increase its horizontal resolution over a region of interest to resolve mesoscale features, while simultaneously simulating (at a lower resolution) the remaining synoptic and global circulation. Hence, it combines the advantages of both GCMs and RCMs. An example of a SGGCM is CAM-EULAG, which is described by Abiodun et al. (2008a) as "… a non-hydrostatic, parallel computational model for all-scale geophysical flows". Abiodun et al. (2008a) shows that stretched grid CAM-EULAG simulations compare favourably, in terms of equatorial wave characteristics, to standard CAM simulations, on an Aqua Planet.

2.3 Wave study over Southern Africa

There is a dearth of academic study on inertial gravity wave activity over Southern Africa. Only a few studies have presented Southern African wave activity as part of wave activity in the equatorial regions (Alexander et al., 2008), global wave observation of potential energy (Namboothiri et al., 2008 and Zhang et al., 2012), or signal to noise filtering of satellite imagery (Eckermann and Wu, 2012).

Alexander et al. (2008) studied waves in the upper troposphere and lower stratosphere equatorial region, and inferred Southern African wave activity from the monthly potential wave energy fields. They found that the minimum wave activity over Southern Africa occurs in January, with decreasing values toward the higher latitudes. They found a localized wave hotspot over southern Namibia in the April that is repeated, but with greater intensity and coverage, in September. Namboothiri et al. (2008) presented four years of global observational wave analysis in the mid-upper troposphere. In the study, wave activity over Southern Africa was dominated by convectively generated waves in austral summer, with a

peak over land in the lower latitudes. The minimum convective activity was in austral winter. Zhang et al. (2012) studied eight years of observational data for wave patterns in the stratosphere. They present global seasonal potential energy behaviour indicating strong wave activity in austral winter in the inertial gravity wave range in the southern parts of the Southern Africa domain. The second highest activity in this region occurs in spring, located south of the continent as well as over central Namibia and Botswana. However, these previous studies showed global activity, in which the regional activity over Southern Africa is coarse. Eckermann and Wu (2012) obtained wave activity with high resolution over Southern Africa, but in the stratosphere, using satellite imagery. However, they draw attention to strong activity zones during austral winter over the Western Cape and Drakensberg topography. This activity is clearly seen beyond the 60 hPa level.

Chapter 3. Methodology

This chapter describes the model, simulation and analysis methods used in the study. A global climate model with grid stretching capability (CAM-EULAG) was applied to simulate the global climate, but with the highest resolution over Southern Africa. The model simulation was validated with NCEP reanalysis data, and analysed to study the characteristics of multi-scale inertial gravity waves over Southern Africa. Variance analysis was used to identify hot spots over the region, Fourier analysis was used to study the energy distribution at various wavelengths and frequency, and Self-Organising Maps (SOMs) were used to identify the spatial character of the waves.

3.1 Model Description and Simulation Set-up

Abiodun et al. (2008a) gives a detailed description of CAM-EULAG. As the name implies, CAM-EULAG (hereafter CEU) is developed from two models: Community Atmospheric Model (CAM, version 3, Collins et al. 2004) and EULAG (Smolarkiewicz and Pudykiewicz, 1992; Smolarkiewicz and Margolin, 1997). CAM is an atmospheric model developed at NCAR (National Centre for Atmospheric Research). EULAG is a non-hydrostatic dynamic core with adaptive grid resolution developed by Prusa and Smolarkiewicz, 2003. CEU combines the dynamic core of EULA with the physics routine of CAM (Abiodun et al., 2008a) and Prusa and Gutowski, 2006. CEU allows for robust atmospheric simulations, while running simultaneously at adaptive resolutions. Areas of focus can be simulated at very high resolutions of up to 1 km, whilst regions outside of the focus domain are simultaneously simulated at lower resolutions. CEU is less computationally intensive and more efficient than uniform resolution grid simulations, thus providing the research community with a powerful high resolution tool that is effective in terms of CPU time. Abiodun et al. (2008a) finds good agreement between stretched grid CEU simulation and standard CAM simulations for equatorial waves on Aqua Planet. The present study uses CEU to simulate the atmosphere in high resolution over Southern Africa in order to resolve mesoscale wave activity.

The model input initialisation of variables: temperature, winds and humidity, geopotential, pressure, sea ice, snow and cloud were derived from standard CAM 3.1 data. These initialisation data were simulated in a five-year spin up of the Community Climate Model

with orbital parameters set at 1950 with a solar constant of 1367 W/m². Ozone was derived from a zonally averaged monthly from Community Climate Model 3 (CCM3). Aerosol Mass was taken from the horizontal interpolation of CAM2.0.2.dev40 data. The Land Surface Model was initiated with output from the Biosphere Atmosphere Transfer Scheme, Global Hydro-graphic Data Release 2.0, Surface land-use types. 0.5x0.5 degree grid, sand, silt, clay dataset from Global Biogeochemical Cycles 7:97-108 and the percentage of grid-cell covered with wetlands (Cogley, 1991). The observed sea surface temperature used in the simulation is from CAM package.

The adaptive grid focused the high resolution over Southern Africa with a horizontal resolution of approximately 0.1° x 0.1° (see Figure 3.1). The remainder of the domain was simulated at a lower resolution of 1.4° x 1.4°.The time step applied in the model was every 20 seconds to satisfy the courant number requirement for high spatial resolution, but the sample rate output of the simulation was hourly. The simulation was run for two climatological years, the first year was discarded as spin-up while the second year was analysed for the study.

3.2 Variance analysis and horizontal wind

The variance in a field is the change in value undergone around its average value (Chandran et al., 2011). The modelling community has extensively used variance analysis to diagnose and present regions of significant variability or to provide a baseline from which other analyses draw (Wu et al., 2010). For this work, horizontal variance analysis (variance in time) of the full domain for each season highlights the areas of peak intensity. In areas where the seasonal variance is high, there is a vertical oscillation about the mean point in the dataset. A larger and more regular oscillation produces peaks in the variance map. In areas where these variance peaks are persistently high compared to the remaining domain in each season, they are defined as areas with potential for heightened wave activity that will be analysed further.

The variance is defined as $\mathrm{Var}(\mathrm{X}) = \frac{1}{\mathrm{n}}\sum_{\mathrm{i}=1}^{\mathrm{n}}(\mathrm{x_i} - \mu)^2$, where *X* is the grid point in the domain, *n* is the number of time intervals and μ is the mean.

3.3 Fourier analysis

Fourier analysis was used to study the energy distribution at various wavelengths and frequencies. Fourier analysis is a classical time series methodology for describing complex multi-harmonic datasets (Priestley, 1981). It allows for the geometric decomposition of temporal or spatial data into multiple sinusoidal components or periodic function (Zwiersand Von Storch, 2004) and the analysis of the spectral characteristics provides the estimated power density of multi-frequency data (Azzali and Menenti, 1999).

The temporal and spatial Fourier analyses are implemented through NOAA Ferret – FFTA function for each season, and areas of persistent high wave activity based on peak variance values in the spatial domain over all seasons for MWZ1 and MWZ2 (see Figure 5.1). The seasonal Fourier values in each high activity zone are averaged and plotted on axes of power against period (between 0.1 and 40 days/cycle) and against wavelength (between 20 and 600 km) for the temporal and spatial Fourier analyses respectively. This dual approach allows for Fourier analysis to capture both migratory wave structure and standing waves that vary in strength.

The classification of inertial gravity waves for this work is defined as waves with a wave-length of between 20 – 300km and with frequencies of 2.4 hours – 10 days. Confirming the activity present in the data as inertial gravity waves would rely on wavelet analysis and determining energy variations for each wave in these ranges. This falls beyond the scope of this work.

Fourier analysis in itself is a measure of oscillatory strength and wave-like consistency present in a dataset. Wave activity for this methodology is roughly defined as the peak deviations from the standard power spectrum against frequency and against wavelength in the Fourier transformation of the vertical wind field for each season. Statistical significance tests of these peaks are not performed, as the data from a single simulated year is very irregular. Only peaks that were clearly present were discussed. These peaks also should be reinforced by a plausible explanation relevant to the season of interest. A multi-year simulation would have presented more defensible statistics.

3.4 Self-Organising Maps

Self-Organising Maps (SOMs) are used to identify the spatial character of the waves from the simulated hourly dataset. Hewitson and Crane (2002) describe the SOM methodology as a means to determine and display the distribution function of a complex multidimensional dataset, whilst treating the data as continuous in time. Node states that they are designed to "minimize the within-group differences while maximizing the between-group differences" (Hewitson and Crane, 2002). A SOM is an artificial neural network algorithm for clustering, abstraction and visualization of complex data (Pearce et al., 2011). SOM output is presented in a regular two-dimensional array (Kohonen, 2001; Pearce et al., 2011). The inter-nodal variability was derived from the training of the SOM on seasonal vertical wind in each domain (Sheridan and Lee, 2011). SOMs are used to capture patterns of vertical wave activity over Southern Africa. The SOM nodes are also presented as vertical cross-sections of the troposphere at 25°S and 32°S for MWZ1 and MWZ2 respectively. (See Figure 5.1)

The applications for SOMs range from downscaling (Crane and Hewitson, 1998), climate classification (Malmgren and Winter, 1998), cloud classification (Ambroisea et al. 2000), synoptic-scale meteorology on air quality (Pearce et al., 2011) to precipitation (Finnis et al., 2009). Sheridan and Lee (2011) observe that the resultant patterns of atmospheric variables with a spatial component can be better understood using SOM analysis and visualisation. Refer to Kohonen (1982, 2001) or Hewitson and Crane (2002) for additional details on SOM analysis.

A wave node in the SOM methodology is defined as any node that exhibits both up and downward motion in either MWZ1 or MWZ2. Wave activity is defined as an oscillation in time and space of the vertical wind field distinct from the surrounding atmosphere. Whether these nodes are exhibiting true wave activity is determined by studying each node's horizontal and vertical wind orientation and cross-sectional properties in isolation.

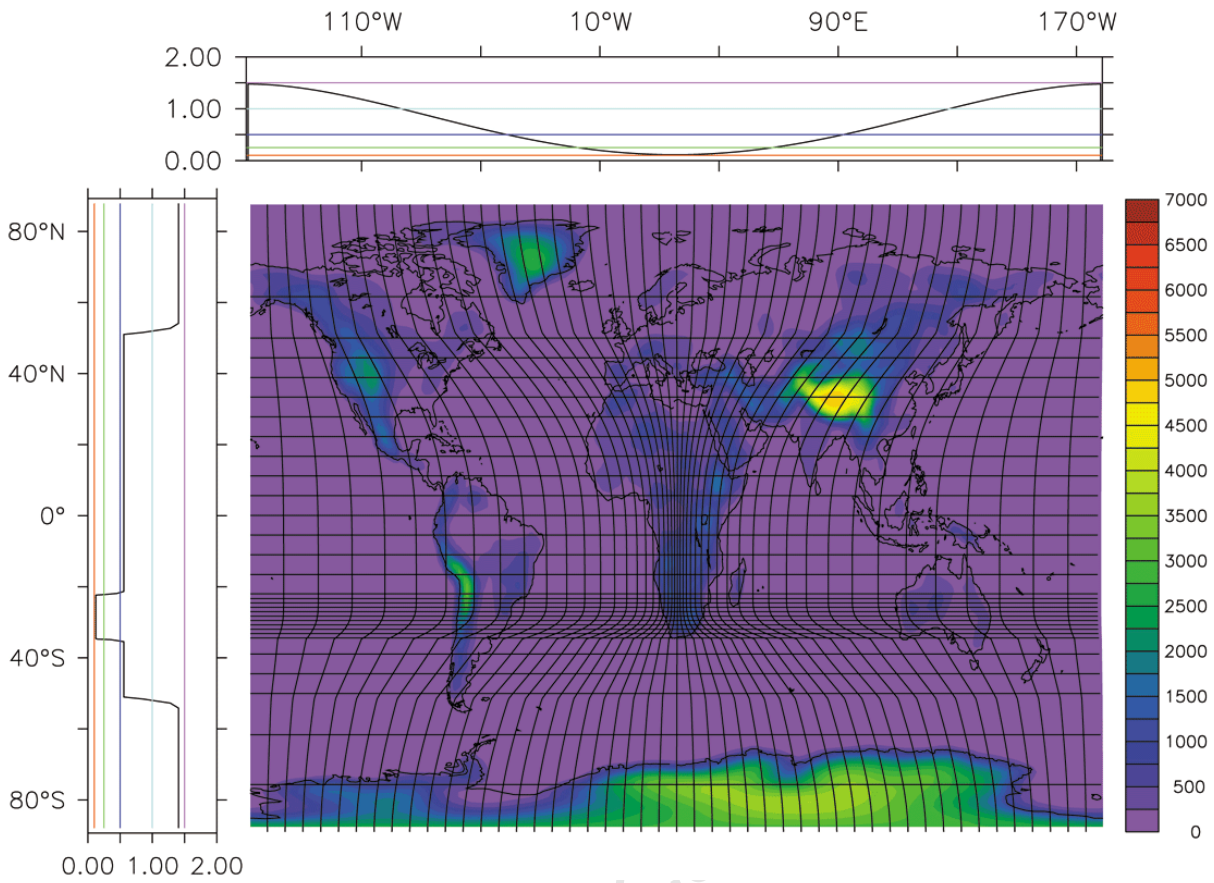

Figure 3.1: Figure shows the topographical input for the model - smoothed height above sea level (m) with the CEU stretched grid depicting high resolution focus over Southern Africa

Chapter 4. Model Validation

4.1 Surface Temperature

There is a good agreement between the simulated global distribution of surface temperatures and the NCEP reanalysis surface temperatures (Figure 4.1). As in NCEP, the simulated surface temperature shows the highest values within the tropics (more than 30°C in both CEU and NCEP), the lowest values at the poles (North Pole in January, and South Pole in June), and the strongest temperature gradient in the mid-latitudes. The simulation also captures the seasonal changes in temperature as depicted in NCEP reanalysis. In both hemispheres, the model shows a warmer temperature over the continents during the hemispheric summer than during the hemispheric winter. The simulated surface temperature patterns over the continents agree well with that of NCEP, especially in January over Australia (around 35°C), in June over Northern Africa (around 40°C), in south western North America (around 35°C) and the over the subcontinent. In general, the magnitude of the simulated temperature is consistent with that of NCEP. The model replicates well the cooling effect of coastal upwelling on surface air over the adjacent oceans west of Southern Africa, northern Africa, South America and North America as in NCEP (Figure 4.1).

Despite these areas of agreement, there are some notable discrepancies between the NCEP and CEU temperatures, especially at the high latitudes. The model shows the highest cold bias north of 75^{o}N, where the model has the lowest horizontal grid resolution; the bias is about 6^{o}C in January and about 4°C in June. In January, whilst the model shows a warm bias (less than 3^{o}C) over Europe, northern Asia and western half of North America, it shows a cold bias over West Africa, southern Asia and eastern half of USA. In June, the warm bias extends over the entire of North America, whilst the cold bias persists over West Africa and India. There is better agreement between the CEU and NCEP temperature patterns over the ocean than over the continents. Another area with a notable difference between CEU and NCEP temperature in January is over in the Himalayan region, where the model shows a warm bias of about 5°C.

However, the model gives a reliable simulation of the regional temperature pattern over Southern African with seasonal variability. In summer (January) the simulated regional

temperature pattern shows high temperatures (>25^{o}C) covering the entire sub-region, but in winter (June) the high temperatures (>25^{o}C) limited to the northern half and eastern coast of the sub-region, are inconsistent with NCEP temperature patterns. Nevertheless, the model shows a warm bias (about 2°C) in the northern and eastern part of the sub-region and a cold bias (about 2°C) over the western part in January and June respectfully (Figure 4.2). The largest disparity between the model and NCEP temperatures is in the south eastern coastal and the northern inland areas.

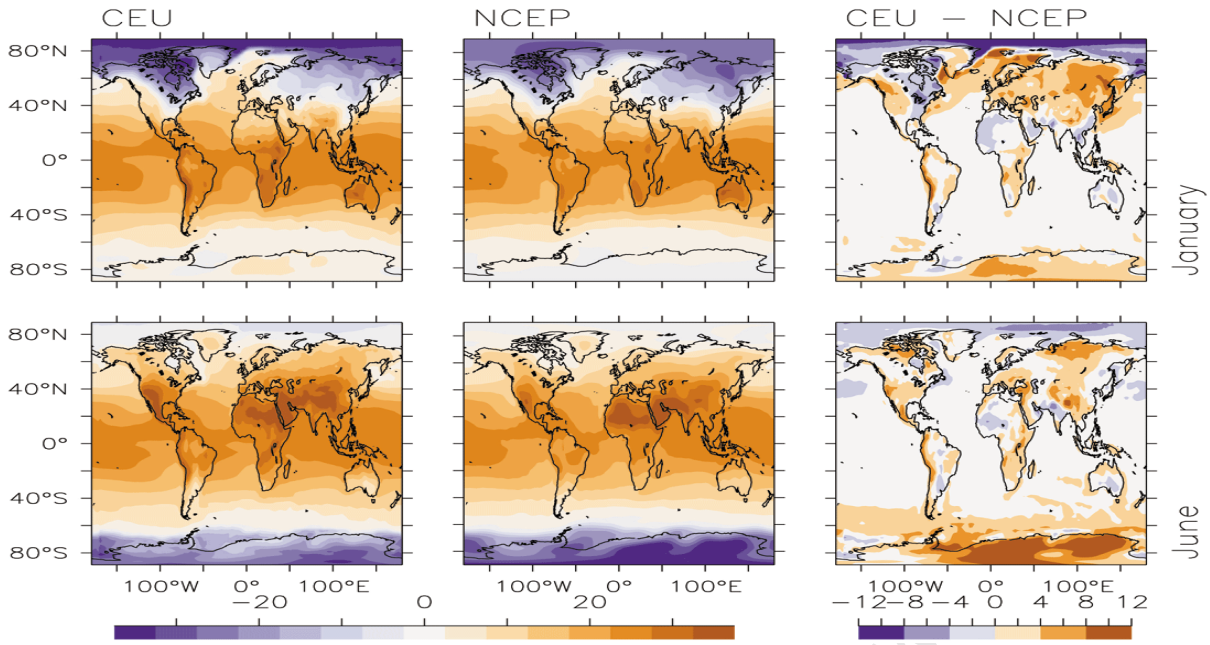

Figure 4.1: Spatial distribution of surface temperature for CEU, NCEP reanalysis, and model bias (CEU – NCEP) in January and June

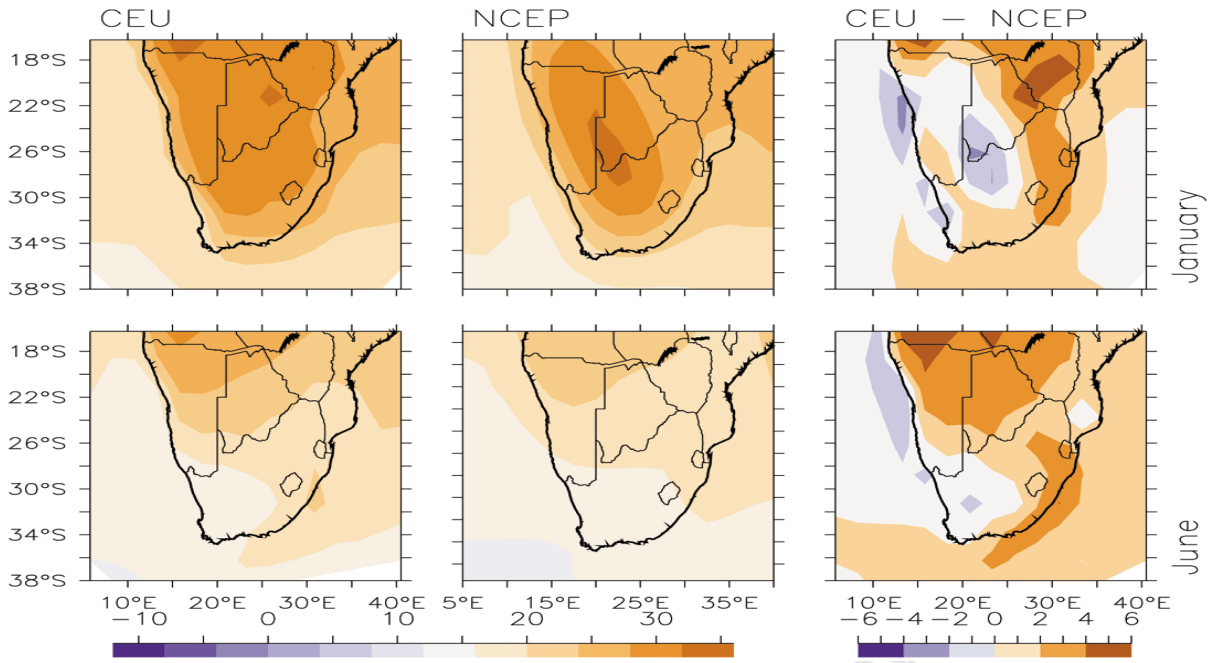

Figure 4.2: Spatial distribution of surface temperature over Southern Africa for CEU, NCEP reanalysis, and model bias (CEU – NCEP) in January and June

4.2 Precipitation

The simulated global precipitation pattern shows a good agreement with that of NCEP, though with some discrepancies (Figure 4.3). Though NCEP precipitation is based on a reanalysis forecast model and as such is not an observed dataset, for consistency of validation it was considered adequate. As in NCEP, the model simulates a band of maximum precipitation (more than 10 mm/day) in the tropics, along the ITCZ, in January and June. The simulated precipitation pattern in the southern hemispheric mid-latitudes agrees well with NCEP, showing a lower precipitation (2 to 3 mm/day) in January than in June (5 to 6 mm/day). In January, the simulated precipitation (about 8 mm/day precipitation) over the northern Atlantic also matches that of NCEP, but with some disagreements in June. The simulated precipitation (distribution and magnitude) over the Indonesian region shows a poor agreement with the NCEP in January and June. However, both CEU and NCEP agree on the non-existent precipitation over the high pressure regions in south Atlantic, south-east Pacific, northern Africa and the high southern latitudes in January and June. In addition, they both show no rainfall in the west of Australia and the eastern half of Asia in January, and no precipitation to the west of USA and over the entire of Australia in June. In general, the model precipitation is lower than that of NCEP along the ITCZ, but higher in Indonesia, Latin America and Southern Africa.

Over Southern Africa, although the CEU rainfall (Figure 4.4) reproduces the seasonal changes in rainfall patterns as in NCEP, there are two obvious biases in the simulated precipitation fields. First, in January, the simulation shows a precipitation bias of 8 mm/day over the central and western part of Southern Africa, where NCEP shows no rainfall. Second, in June, the simulation shows precipitation over most of South Africa and over the ocean, whereas NCEP shows no precipitation over land, but only over the southern and eastern oceans. Hence, the model generally shows a wet bias over Southern Africa in January and June. This wet bias could be due to the convective parameterization schemes that have not been fine-tuned for the high resolution simulation used in the study. However, the simulation of a rainfall peak over the western part of Southern Africa, instead of the eastern part, in June is a generic problem with CAM (on which CEU was developed), as similar errors are present in previous studies with CAM (Collins et al., 2006).The simulated wet bias over the western part of Southern Africa in January is consistent with the cold bias over the region, because the

higher rainfall implies higher soil moisture, lower sensible heat flux and hence lower temperature. The higher soil moisture could also have a positive feedback on rainfall through the enhanced evapotranspiration.

A look at the simulated wind field suggests that the rainfall bias may be linked to the transport of moisture over the sub-domain (Figure 4.4). In January, the simulated wind is anti-clockwise over the continent, which is in agreement with the NCEP, whilst the simulated easterlies are stronger than those of NCEP over the Indian Ocean, northern South Africa and southern Botswana. Hence there is greater transportation of moisture from the Indian Ocean over the western part of the sub-region in the simulation, which produces higher rainfall than in NCEP.

There is another discrepancy between the simulated and NCEP wind fields in January that can also contribute to the wet bias over the western part of the Southern Africa. Over this area, CEU simulates a warm, moist northerly flow, which induces surface convergence and enhances rainfall, but NCEP shows a cold, dry southerly flow, which may induce surface divergence and suppress rainfall. Over the adjacent Atlantic Ocean, the model simulates easterly flows, but NCEP shows a southerly flow. In general, the model extends the southern Atlantic anti-cyclonic flow, whereas NCEP extends the southern Indian Ocean anti-cyclonic flow over Southern Africa. In June, there is a better agreement between the simulated and NCEP flow pattern, except that the model produces a stronger north-easterly flow over the sub-continent, and the flow presents a stronger convergence with the westerly flow (and produces more rainfall) over the southern part of South Africa.

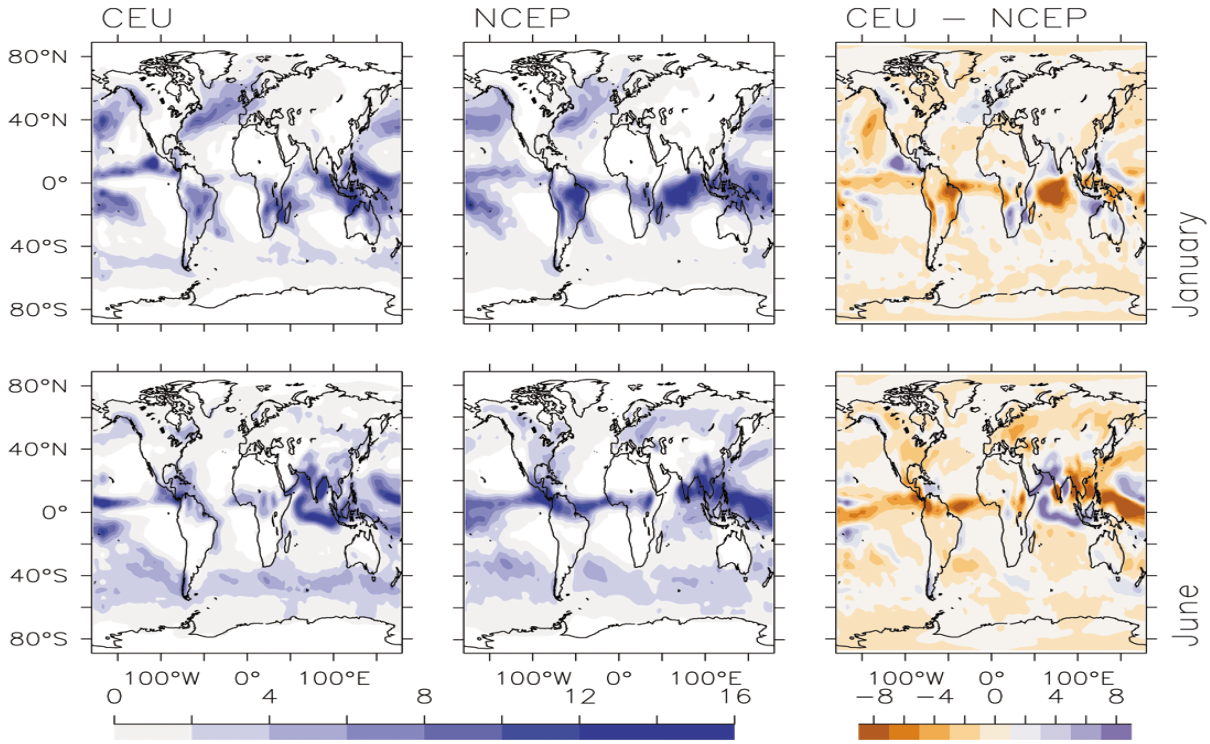

Figure 4.3: Spatial distribution of precipitation (mm/day) for CEU, NCEP reanalysis, and model bias (CEU – NCEP) in January and June

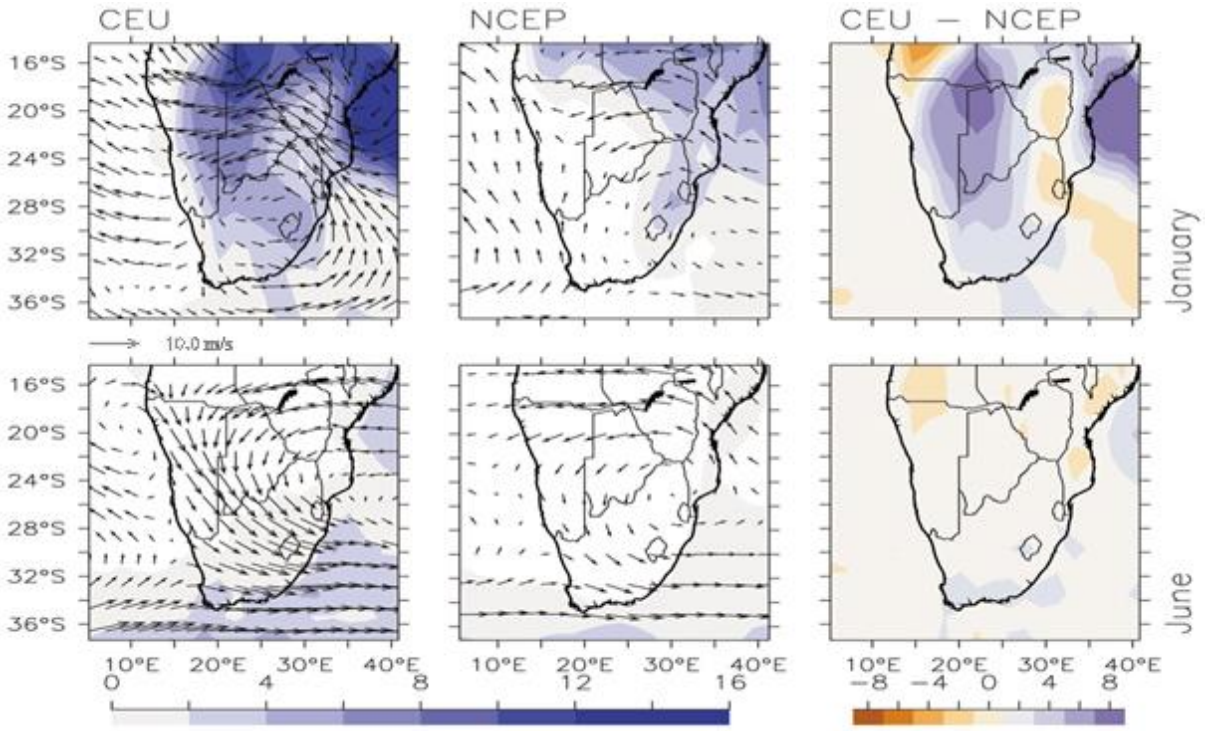

Figure 4.4: Spatial distribution of precipitation (mm/day) and wind at 850hPa over Southern Africa for CEU, NCEP reanalysis, and model bias (CEU – NCEP) in January and June

4.3 Vertical wind velocity

On a global scale, the simulated vertical wind fields at 700hPa show a good agreement with NCEP, though with a few discrepancies (Figure 4.5). The simulated vertical wind fields are well coupled with the rainfall and horizontal wind fields; for instance, the regions of sinking air west of the continent are dry, while the regions with upward motions are wet. In the simulation, the regions of upward motion along the ITCZ (Figure 4.1) over oceans and continents are the same as those in the NCEP. The subsidence motions, associated with high pressure systems (i.e. the downward arm of Hadley and Ferrell cells), are well positioned and are influenced by changes in season, as in NCEP. In June, the high pressure systems over the southern oceans shift towards the equator in both NCEP and CEU. However, the magnitude of the simulated vertical wind is stronger than that of NCEP, resulting in stronger vertical wind gradients between areas with upward motions and subsidence. This is apparent in January over western North America, where the magnitude of the subsidence motion is 0.06 Pa/s in NCEP, but 0.09 Pa/S in CEU; between northern Africa and the equatorial Americas the vertical motion is 0.03 Pa/s, but 0.05 Pa/s in CEU.

The simulated vertical velocity over Southern Africa shows a reasonable agreement with that of NCEP, but with some discrepancies (Figure 4.6). In January, CEU and NCEP show a strong upward motion (about 0.08 Pa/s) over land and downward motion (about 0.08 Pa/s) over the Atlantic Ocean. However, the maximum strong vertical motion is located over the western half of Southern Africa in NCEP, but over the central region of Southern Africa in the simulation. The maximum bias in the simulated vertical motion is ±0.6 Pa/s and occurs in the tropical region. Both NCEP and CEU show that the upward motion over the continent is weaker in January than in June. While NCEP shows that the subsidence motion over the South Atlantic Ocean is weaker in June than in January, CEU simulates the subsidence equal strength in both months. However, the agreement between CEU and NCEP is better than in January.

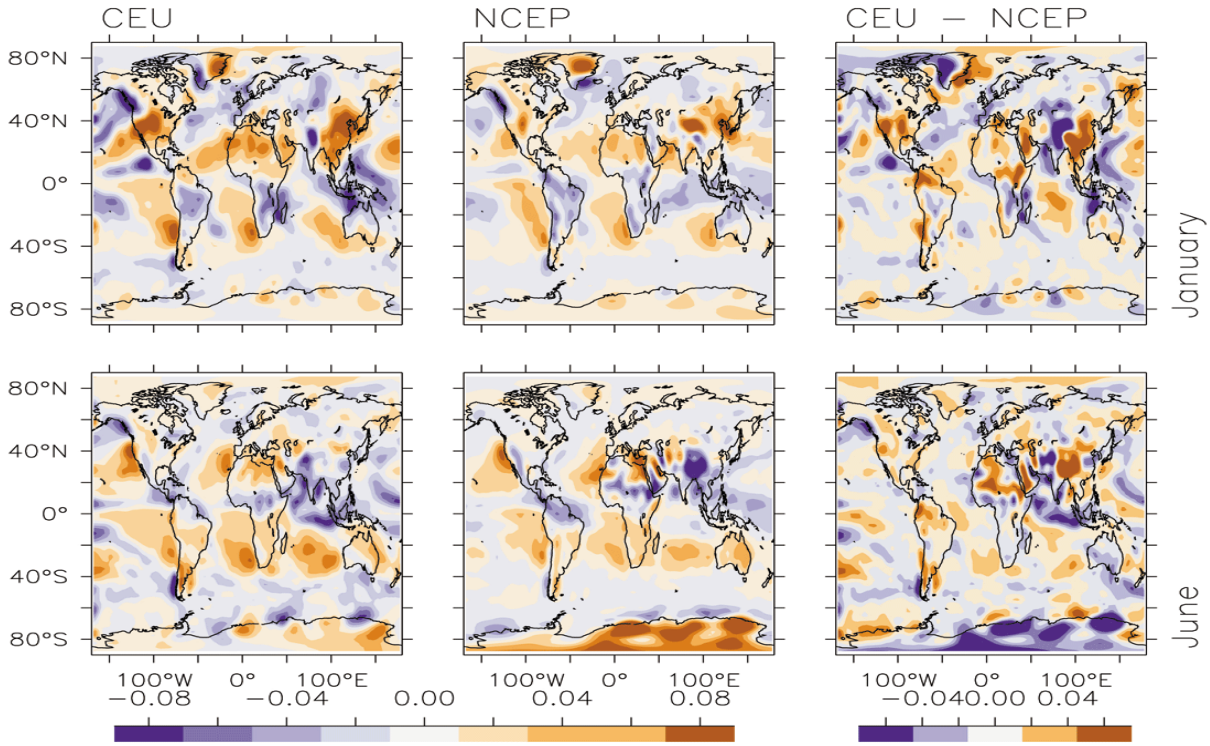

Figure 4.5: Spatial distribution of vertical wind speed (Pascal/s) at 750 hPa for CEU, NCEP reanalysis, and model bias (CEU – NCEP) in January and June

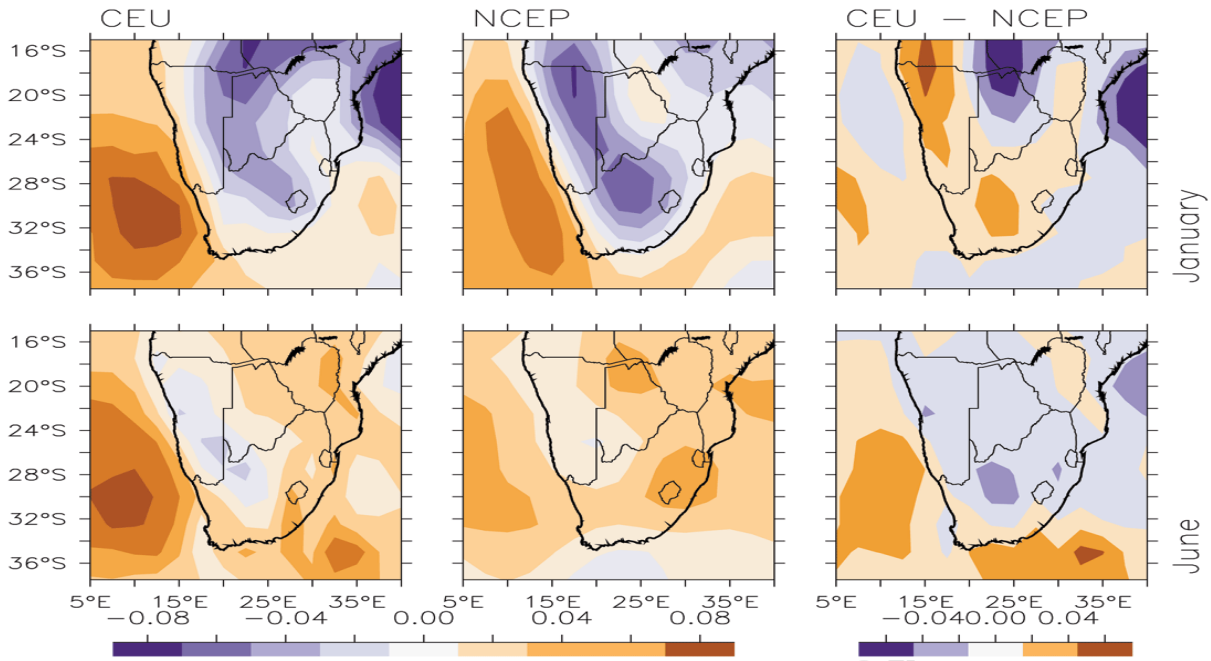

Figure 4.6: Spatial distribution of vertical wind speed (Pascal/s) at 750 hPa over Southern Africa for CEU, NCEP reanalysis, and model bias (CEU – NCEP) in January and June

Chapter 5. Characteristics of simulated inertial gravity waves

This chapter presents the characteristics of the multi-scale waves over Southern Africa as simulated by CEU. It starts by identifying zones of strong wave activities over the domain, then discusses seasonal changes in the location and intensity of vertical wind in the zones, examines spectral characteristics (frequency and wavelength) of the wave activities in the zones, and studies the SOMs classification of vertical motion of each zone into groups. The variance of vertical wind component was used to indentify persistent wave activities.

5.1 The Spatial Distribution

The variance of the simulated vertical wind at 850 hPa shows three zones of maximum wave activities over Southern Africa (Figure 5.1). The first zone (hereafter, MWZ1) is located over the southern Kalahari Desert; the second zone (hereafter, MWZ2) is over the eastern coast of South Africa (and extends over the South Indian Ocean); and the third zone (MWZ3) is over the southern part of the Western Cape. The wave characteristics of these zones vary with the seasons. With MWZ1, in DJF, the activity centers on 28^{o}S, 20^{o}E with a north-west – south-east orientation, and extends from 32^{o}S to 22^{o}S in meridional direction and from 15^{o}E to 23^{o}E in the zonal direction. In MAM, the wave activity becomes stronger and broader as variance increases (by about 1.0 cm/s) to 2.8 cm/s, and its eastward boundary extends (by about 2^{o}) to 25^{o}E. In JJA, the strength, orientation and size of the wave activity are the same as in MAM, but the centre of the wave activity shifts (by 2^{o} eastward) to 22^{o}E. In SON, the wave activity has a zonal orientation and extends in a south-easterly direction to merge with those in MWZ2. The seasonal changes in wave activity simulated here are consistent with results of Alexandra (2008), who observed that gravity wave activity in the stratosphere over Southern Africa is weak in January but stronger and broader in September.

With MWZ2 (Figure 5.1), the wave activity extends from 24^{o}E to 36^{o}E and from 36^{o}S to 26^{o}S. The location and area covered by the wave do not change considerably with seasons, but the strength changes with the season. The strongest activity and highest variance occurs in JJA and the weakest is in DJF. This is in agreement with Zhang et al. (2012), who showed

seasonal wave potential energy over the southern part of South Africa has the maximum peak during winter, followed by spring, autumn and lastly summer. The authors suggested that topography and deep convective activity are significant sources of wave activity.

With MWZ3, the wave activity, which only exists in JJA and SON, centers over the Cape Town region (33^{o}S, 19^{o}E) and extends from 36^{o}S to 34^{o}S in the meridional direction, and from 15^{o}E to 23^{o}E in the zonal direction, merging with MWZ2. However, the MWZ3 wave activity is not of interest to the present study. The focus of subsequent discussion will be on the wave activities in MWZ1 and MWZ2.

The formation and seasonal changes of these zones can be attributed to meso-scale and synoptic atmospheric processes (i.e. convection and frontal systems). However, the consistency with which these two zones show the greatest variance suggests that seasonal factors play only a part of the vertical forcing. Orography seems to play an important role because the location of these zones are over (or near) mountain ranges in Southern Africa. It is possible that while MWZ1 owes its formation to a combination of convective (moist or dry) and orographically induced vertical motion, MWZ2 seems to owe its formation to the interaction of large-scale (inertia) wave interaction with topography. i.e. the interception of horizontal wind by the mountains produces the vertical motions that define the location of the zones.

As a study of the prevailing mean synoptic conditions around the zones, Figure 5.2presents the wind flow at 850 hPa. In summer (DJF), the wind fields show a weak anticyclonic flow over Southern Africa; the centre of the cyclonic flow is at Gauteng (around 26^{o}S, 29^{o}E). The anticyclonic flow features weak northerlies (to north-westerlies; about 2m/s) in MWZ1 and westerlies (about 8.0 m/s) over MWZ2. The wave activity presented in MWZ1 in summer seems to be primarily due to convective activity. Results from troposphere analysis presented by Namboothiri et al. (2008) show a strong variance, filtered particularly for convective excitement, over the MWZ1 area in DJF and weaker activity during JJA, in agreement with our findings. The weaker winds in this season (when compared to any other season) may be the reason why the wave activity in the zones is weaker than any other season. In the other months MWZ1 is dominated by stronger north-westerly flows (about

10.0 m/s) which transport moisture from the tropics. In MWZ2, wind speed is greater than 10 m/s and is dominated by north-westerlies in MAM, but by westerlies in JJA and SON. These seasons also show the strongest variances in MWZ2.In a study focusing on Southern African wave activity from satellite imagery, Eckermann and Wu (2012) confirm the source of this wave activity as orographic. They depict winter as the season with the peak activity. Furthermore, they highlight areas exhibiting strongest wave activity to the east of the Drakensberg range (MWZ2), the Groot Karas Mountains (MWZ1) and the Cape Fold Belt (MWZ3).

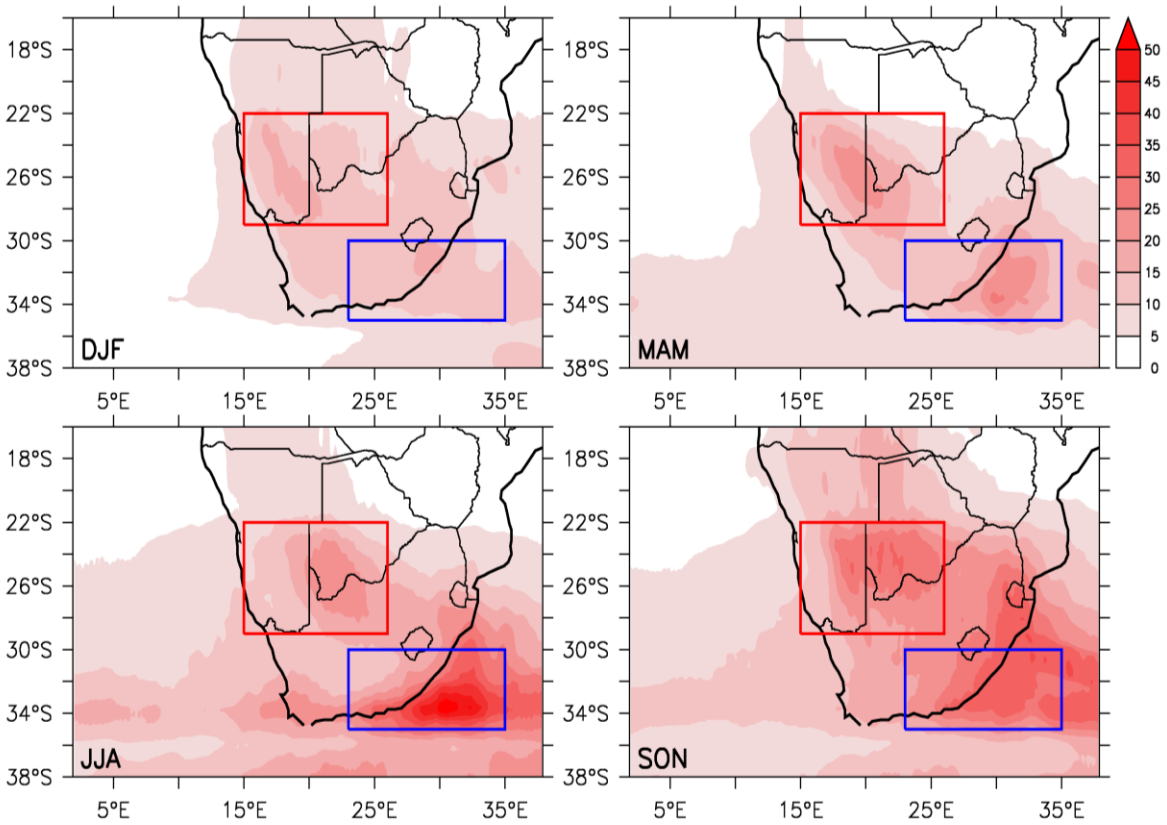

Figure 5.1: Variance of vertical wind at 850 hPa level in DJF, MAM, JJA and SON. Regions of strong wave in all the seasons are MWZ1 and MWZ2 indicated with red and blue rectangles respectfully.

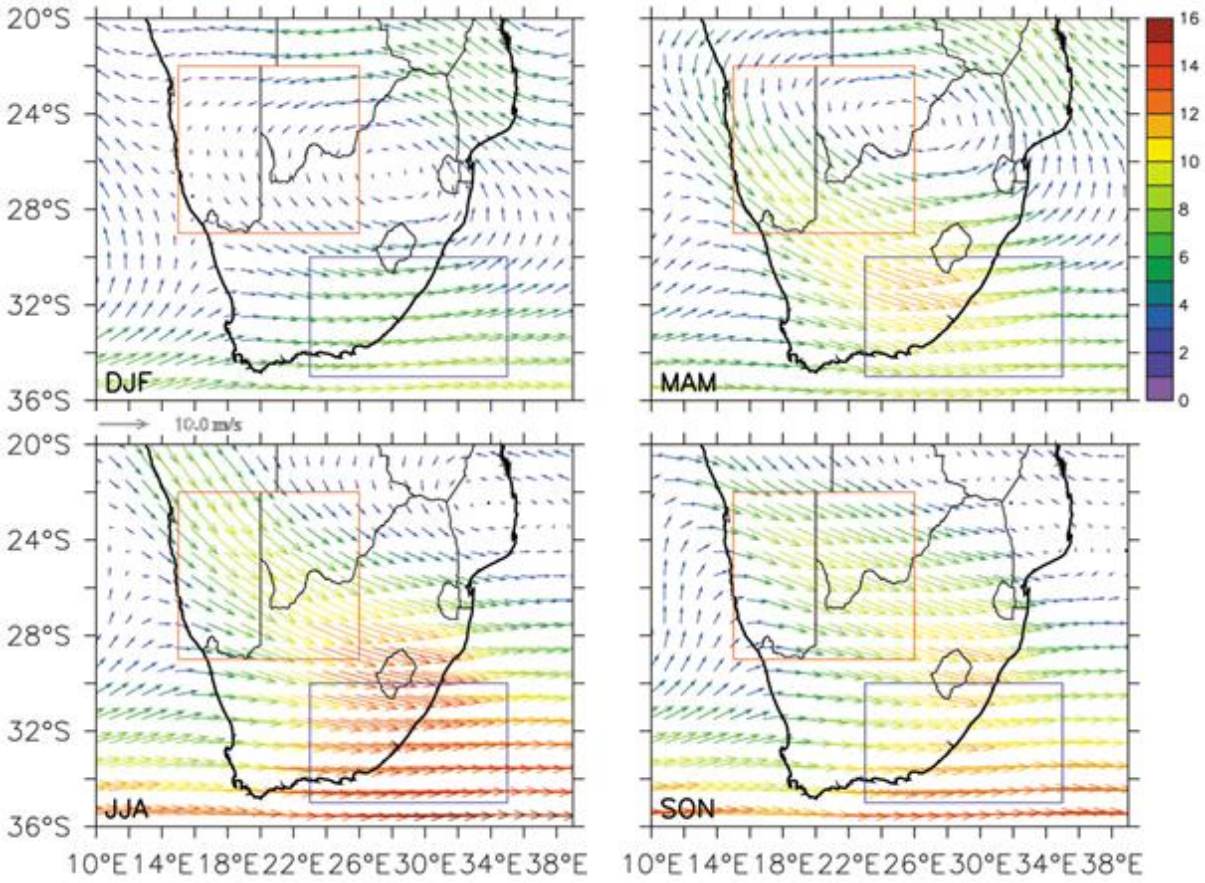

Figure 5.2: The CEU 850 hPa synoptic wind flow over Southern Africa in DJF, MAM, JJA, and SON. The colour indicates the wind speed (m/s). The areas of focus are indicated with rectangles.

5.2 The Power Spectrum - Temporal

Fourier used spectral analysis (power against period) to express wave characteristics in the zones MWZ1 and MWZ2, shown in Figure 5.3 and Figure 5.4. The power spectrum was calculated from the Fourier analysis of hourly data and showed MWZ1 having three distinctive peaks in DJF (at 0.5, 1.0 and 9.0 days), in MAM (at 0.5, 1.0 and 5.0 days), and in SON (at 1.0, 3.0 and 5.0 days); no peaks in JJA. The power spectrum for MWZ2 shows peaks in DJF (at 0.5, 1.0, 3.0 and 9.0 days), in MAM (at 0.5, 1.0 and 5.0 days), and in SON (at 1.0, 3.0 and 5.0 days).In JJA, the MWZ2 show no peaks but rather shows a general increase in strength in the 3.0- to 6.0-day range.

The 0.5- and 1.0-day peaks seem to represent vertical motion generated by semi-diurnal local scale processes, like thermally induced topographic processes such as up-slope and down-slope winds, katabatic and anabtic winds, or by diurnal processes such as convection (dry or moist). Sub-daily peaks are present only in the warmer thermally active seasons of DJF and MAM. However, 0.5- and 1.0-day oscillations, which are probably caused in other seasons by the diurnal cycle, are absent in winter period (JJA). On the other hand, the 3.0 – 10-day wave peaks appear to represent the vertical motion-induced synoptic scale activities like the easterly waves, TTT system (dominating in SON), the ITCZ (dominating in SON and DJF) or frontal activity (dominating in JJA) and are present, to a varying degree, in each season (excluding JJA in MWZ1).

In general, energy rapidly decreases from the low frequency range (long period) to the high frequency range (short period). This suggests that energy is transferred from lower frequencies by non-linear processes and the energy will be eventually lost as heat by viscosity at much higher frequencies. This same conclusion is reached by Dalin et al. (2012) in their spectral analysis of inertial gravity waves. Their results show a decreased spectral power with a decrease in wave period, in line with the power law, as is also noted in both Figure 5.3 and Figure 5.4 of this work. Their Fourier analysis revealed peaks at the 4-hour and 0.5-, 1- and 3-day periods. Analysis of short periods presents highly variable strength, in line with analysis in this work.

There is a notable difference between the slopes of the power spectral at higher frequency; the slope of the JJA power spectral in both MWZ1 and MWZ2 is weaker than those of other seasons. In addition, the power spectral slope is distinctly shallower in MWZ2 than in MWZ1. This indicates that the rate of energy transfer in those frequency ranges is slower in JJA than in other seasons. It is likely that this is caused by increased mixing during the winter months (exhibiting strong winds). The slope of DJF (when winds are weaker) is sharper for both MWZ1 and MWZ2. The average strengths of the power spectral over MWZ1 are 0.0416, 0.0306, 0.0303 and 0.02478, in SON, MAM, JJA and DJF respectively.

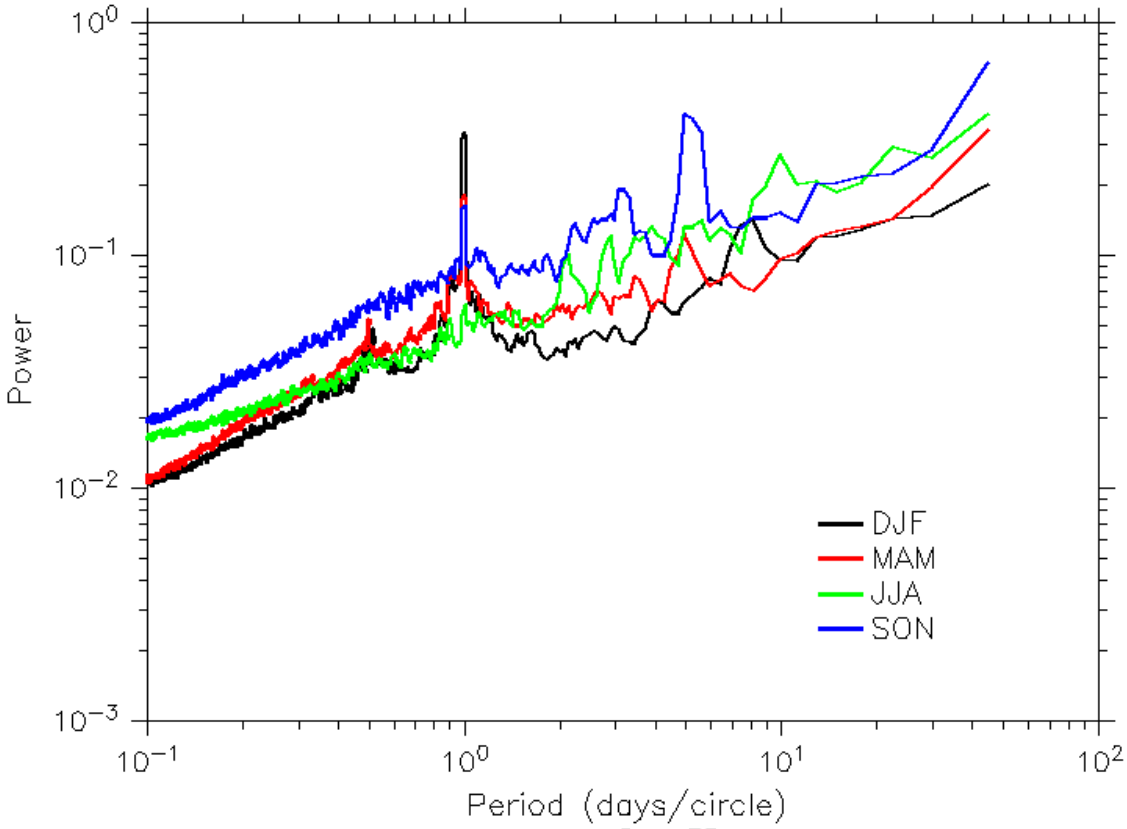

Figure 5.3: The variation of wave activity with frequency (Power Spectrum) in MWZ1 during DJF, MAM, JJA and SON.

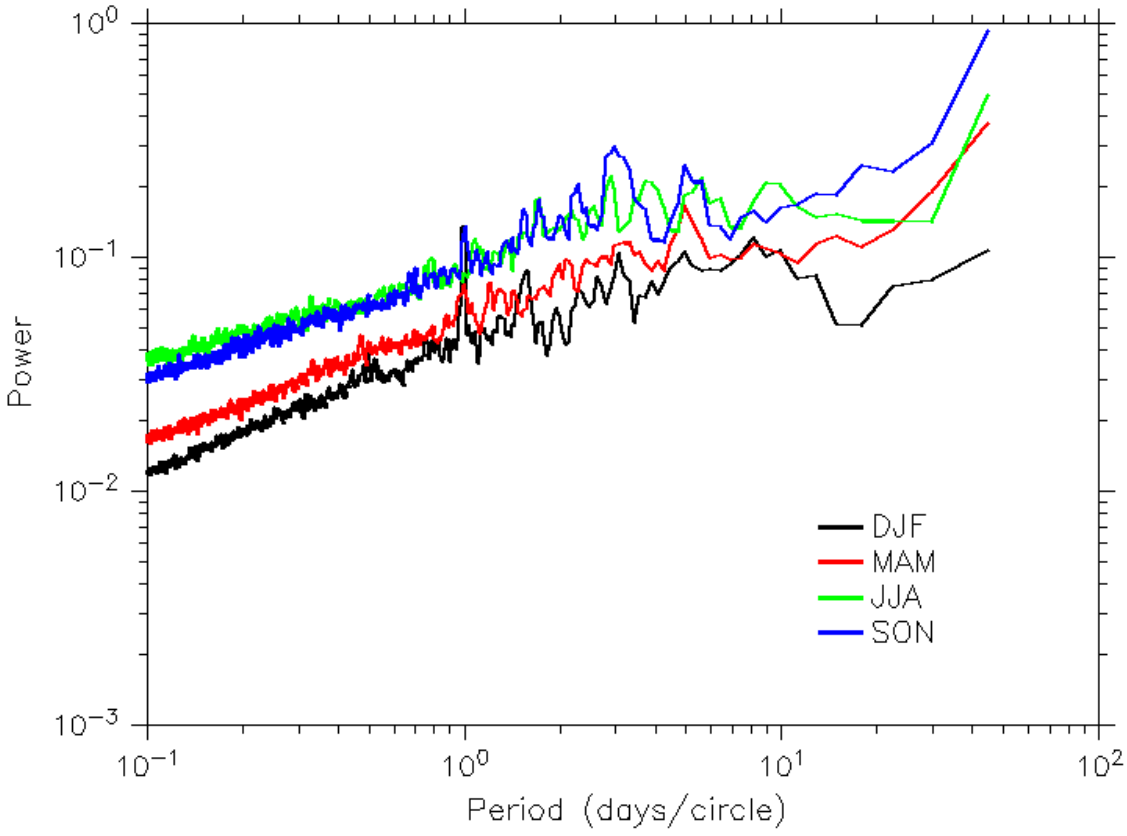

Figure 5.4: The variation of wave activity with frequency (Power Spectrum) in MWZ2 during DJF, MAM, JJA and SON.

5.3 The Power Spectrum - Spatial

Figure 5.5 and Figure 5.6 present the power spectrum against wavelength to further describe the characteristics of the wave activity in zones MWZ1 and MWZ2. The power spectrum is calculated through the use of a transverse Fourier transformation of the 850 hPa vertical wind field measuring wave patterns over 10 km through time. The spectral analysis of wavelength in MWZ1 does not show any discernible peak. In agreement with the atmospheric power law, the analysis presents a smooth profile with stronger values at the longer, synoptically dominated wavelengths (more than 100 km), sharply decreasing strength between 100 km and 40 km in the meso-scale and weak at the local scale wavelength (less than 40km). SON consistently shows the greatest strength over the entire wavelength range. Summer (DJF) shows weaker strength at the longer wavelengths but is stronger than SON at the local scale. MAM remains weaker but has a curve similar to the SON months. The power wavelength curve is however different in winter, as strength is somewhat retained in the longer wavelengths in JJA and is on par with the meso-scale data shown in SON. The lower wavelengths show a decreased strength.

Strength at the local wavelengths, as shown in SON and DJF, may represent the convective activity in warmer seasons. The colder months of MAM and JJA do not express this same strength. In the meso-scale, SON and JJA express similar strength, with MAM and DJF showing weaker activity. At the larger scale, strength in JJA is diminished and is on par with MAM and DJF.

In Figure 5.6, MWZ2 - the power spectrum shows a peak in the activity peak at local and meso-scale in all seasons and represents the wave activity excited by local factors such as upwind topography. Between 60 and 100 km, the strongest wave activity is stronger in SON than JJA. There is a decrease in wave activity at wavelength 50 km, followed by a sharp increase for the longer synoptic wavelengths in all seasons. Since MWZ2 is located south of MWZ1, and has less land cover than MWZ1,the influence of its convection on the wave activity is less in MWZ2 than in MWZ1 (as seen in DJF), but the influence of the frontal system on the wave activity is seemingly more in MWZ2 than in MWZ1 (JJA).The increase in power spectral strength toward the longer wavelength is characteristic of the atmospheric-power law in the inertia sub-range, where the energy is transferred from high frequency.

This is discussed by Allen and Vincent (1995), who show a decrease in spectral strength with increasing wave number (or decreasing wavelength) observational data.

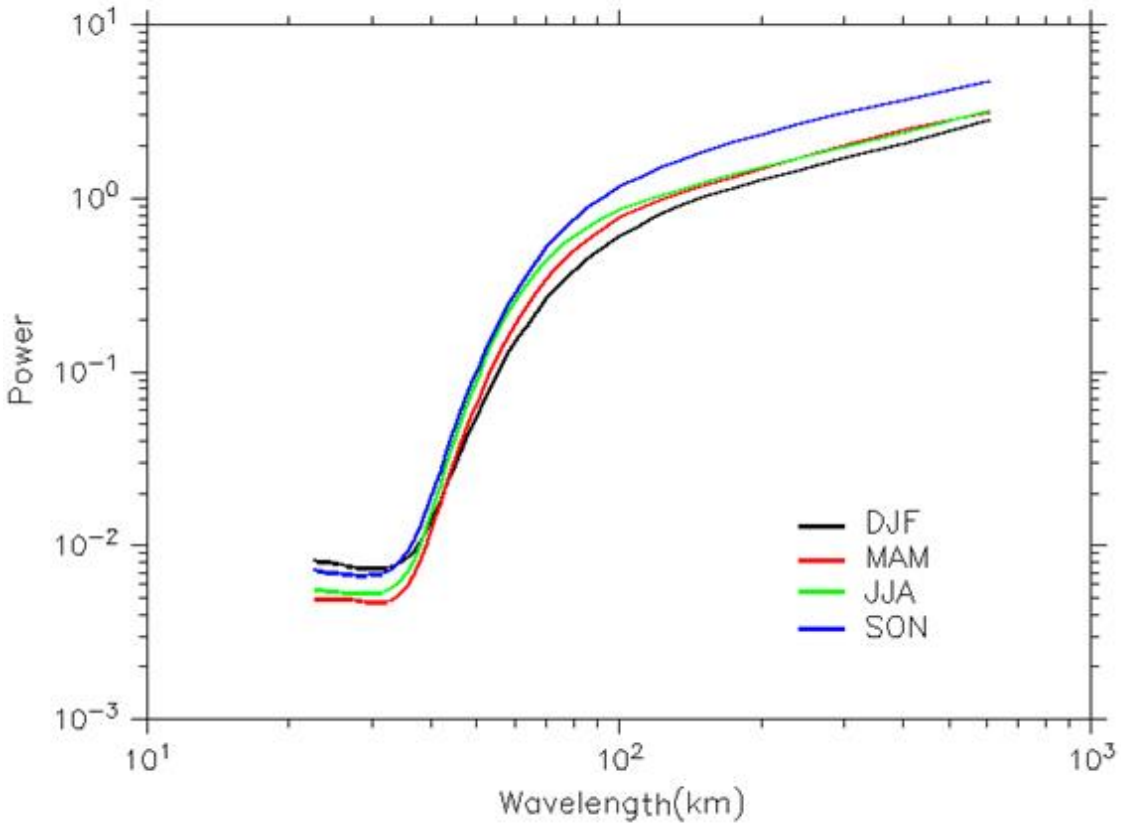

Figure 5.5: The variation of wave power with wavelength in MWZ1 during DJF, MAM, JJA and SON.

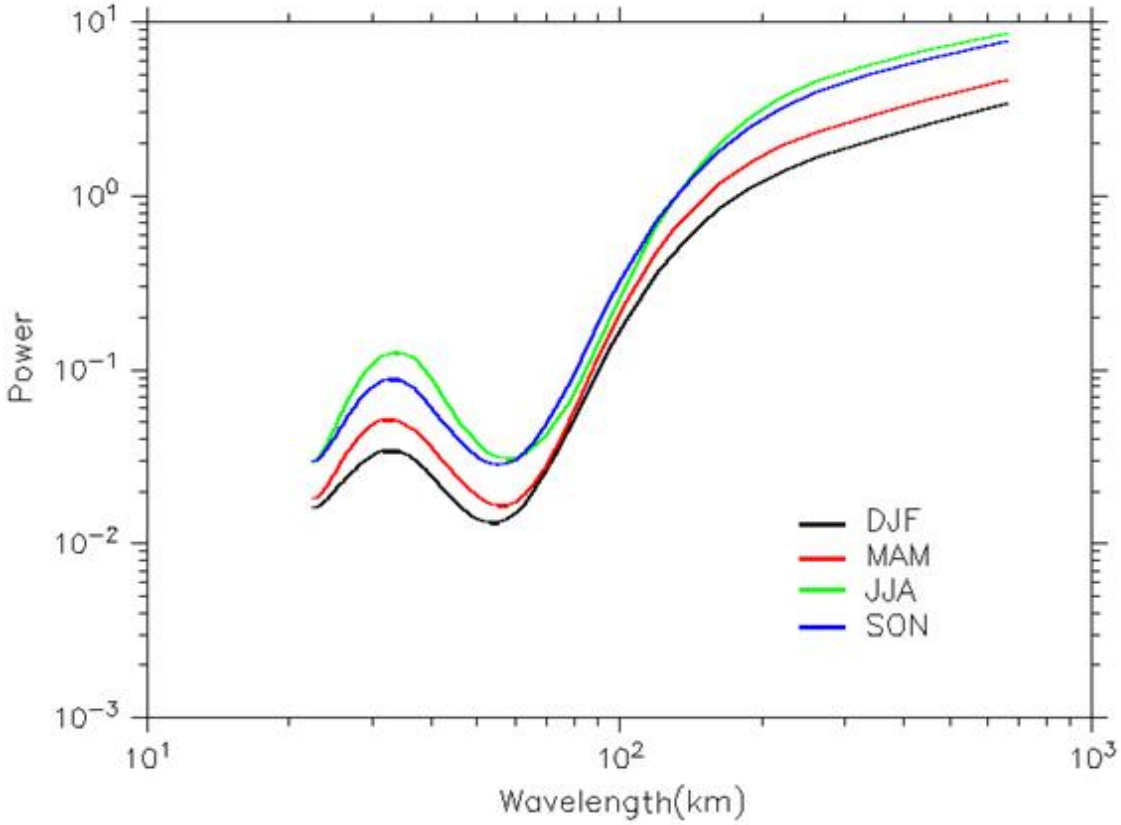

Figure 5.6: The variation of wave power with wavelength in MWZ2 during DJF, MAM, JJA and SON.

5.4 Classification of wave activities with Self Organising Maps

Figure 5.7 to Figure 5.22present results of SOMs analysis. The figures show 16 nodes that typify different vertical wind patterns over the two zones (MWZ1 and MWZ2) in the four seasons (DJF, MAM, JJA, SON). The SOM was trained on the hourly 850 hPa vertical wind level for each three-month seasonal period. The frequency of occurrence of each pattern is indicated on the bottom right of each node. The horizontal wind vectors are an average of the hourly winds corresponding to each instance of vertical wind matching a particular node in the SOM. The meridional cross-section depicts the same nodes, but now the vertical structure of the troposphere at 25°S (MWZ1) and 33°S (MWZ2). Here, we discuss the characteristics of SOM nodes for each zone and season. For an easier discussion, we shall classify the nodes into two groups: wave nodes and non-wave nodes. A wave node is a node that has wave patterns; that is, the node has both positive (upward, blue) and negative (downward, orange) vertical velocities occurring simultaneously within the horizontal domain. A non-wave node, on the other hand, is a node that does not show a wave pattern. The emphasis of our discussion, however, shall be on the wave nodes.

With MWZ1, the analysis shows that the numbers of wave node and non-wave vary with seasons. In DJF (Figure 5.7), 12 nodes (out of the 16 nodes) are wave nodes; the remaining four nodes are non-wave nodes [i.e. Nodes (1),(2),(5),and (6)]. The wave nodes account for more than 67% of the dataset for this season. Nodes (13), (16) and (4) show the extreme patterns in the wave nodes. Node (16) shows a strong upward motion extending from the north-west corner to the south-west corner, and two downward motions running parallel (to the upward motion) on either side at the north-eastern and south-western corners; however, the strength and size of the upward motion is more than both the downward motions.

The vertical motion is associated with a north-westerly wind from an anti-cyclonic flow. In Node (4), the upward motion occupies the south-west half of the domain, while the downward motion occupies the north-eastern part. In Node (13), the reverse of the activity shown in Node (4) is the case: the upward motion occupies the north-eastern part and the downward motion the south-west. The other wave nodes show transition patterns between Node (16) and Node (13), or Node (16) and Node (4). Nodes (13) to (15) have very weak

westerly horizontal wind and show upward motion on the eastern part of the domain associated with convective activity (Figure 5.8). Nodes (4), (8), (11), (12)show a similar pattern to Node (16) but with a weaker upward motion. Generally, in the wave node, an anti-cyclonic flow is shown to produce westerlies on the western half of the domain and easterlies on northern half; however, the anti-cyclonic flow is strongest in Nodes (4), (8), (12), and (16).Figure (5.8) indicates that the vertical motion in these nodes can be associated with topography. The easterly flow sinks as it descends the plateau, while the westerly flow rises as it ascends the plateau, riding over the easterly one. The non-wave nodes show a downward motion occupying the entire domain, with the strongest motion at western side of the plateau where the easterly flow descends the slope.

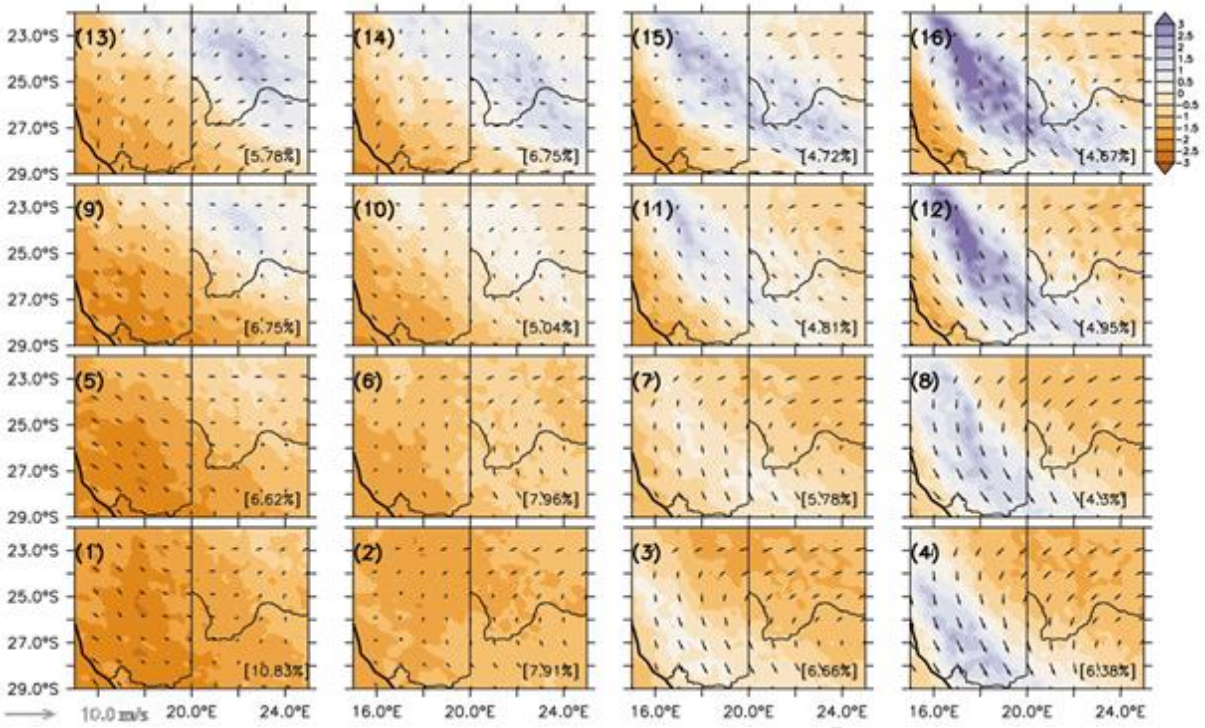

Figure 5.7: The SOM array of 850 hPa vertical wind (cm/s) in Summer (DJF) over MWZ1 zone. Each node represents a synoptic vertical wind pattern over the MWZ1 zone. Negative value indicates downward motion and positive value indicates upward motion. The associated horizontal wind flows (m/s) at 850 hPa are indicated with arrows.

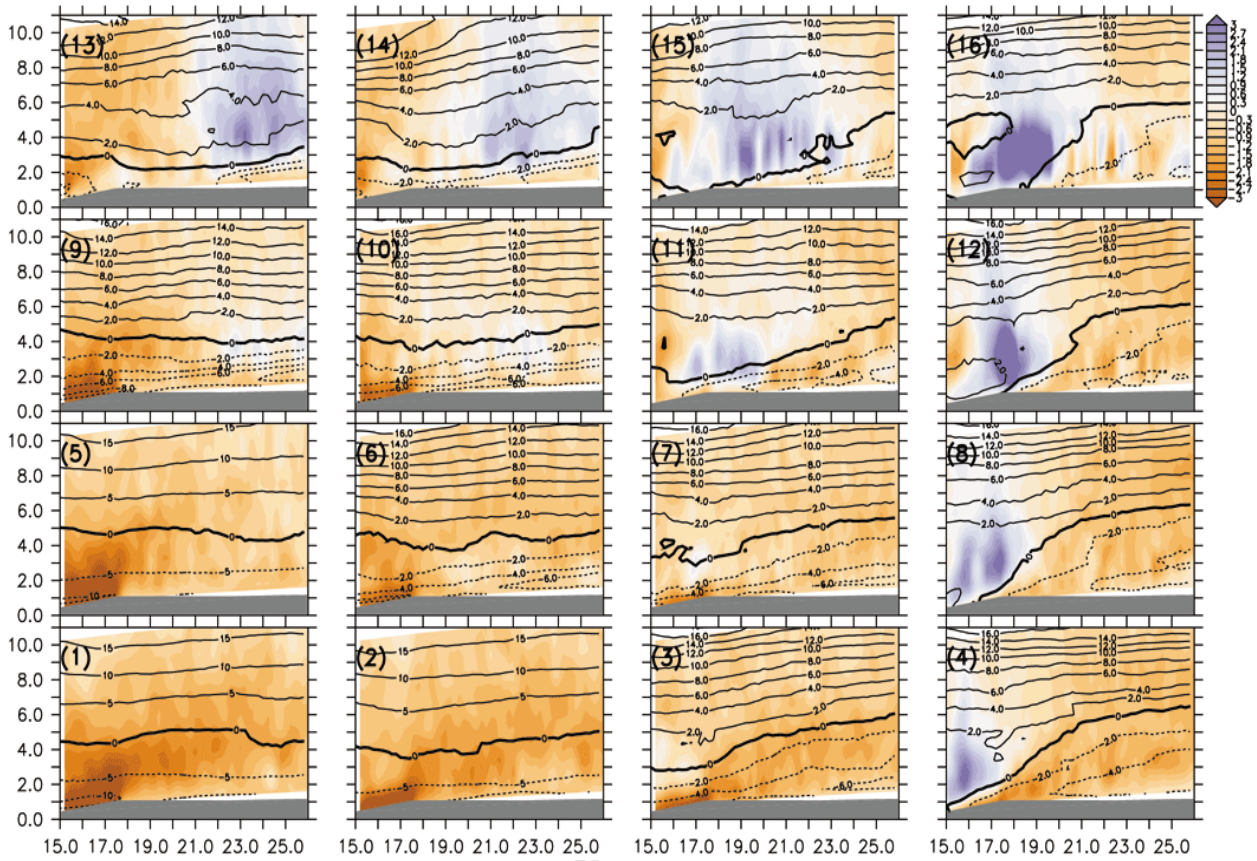

Figure 5.8: The corresponding vertical cross-section of vertical velocity (cm/s; colour) and zonal wind (m/s; contour) for the SOM array shown in Figure 5.7. The values are obtained at latitude 25°S. The topography is indicated in grey. In vertical velocity, negative value indicates downward motion and positive value indicates upward motion. In the zonal wind, negative value (i.e. dashed contour) indicates easterly flow and positive value indicate westerly flow.

In MAM, the MWZ1 is dominated by non-wave nodes (Figure 5.9). There are only four wave nodes [Nodes (1), (5), (9), and (13)] and they account for less than 22% of the dataset. The wave nodes show a strong upward motion running in the north-westerly to south-easterly direction at the centre of the domain and a subsidence motion to the south-west corner of the domain. However, the strength of the vertical motions are stronger in Nodes (1) and (5) than in Nodes (9) and (13). The strength of the upward motion is stronger in Node (5) than Node (1). In non-wave nodes the upward motion dominates. Given that this is a summer season, the upward motions are probably induced through convection.

All the nodes feature a strong anticyclonic flow and the north-westerly wind arm of the anti-cyclone also produces upward motion as it climbs the plateau (Figure 5.10). But the horizontal wind is stronger in the non-wave nodes than in the wave nodes. In Node (4), the upward motion is at the centre of the domain. In Nodes (8), (12), and (16) the peak of the upward motion is located south-west of its position in Nodes (4). The reverse is the case in Node (2); the peak of the vertical motion is located north-east of Node (4).

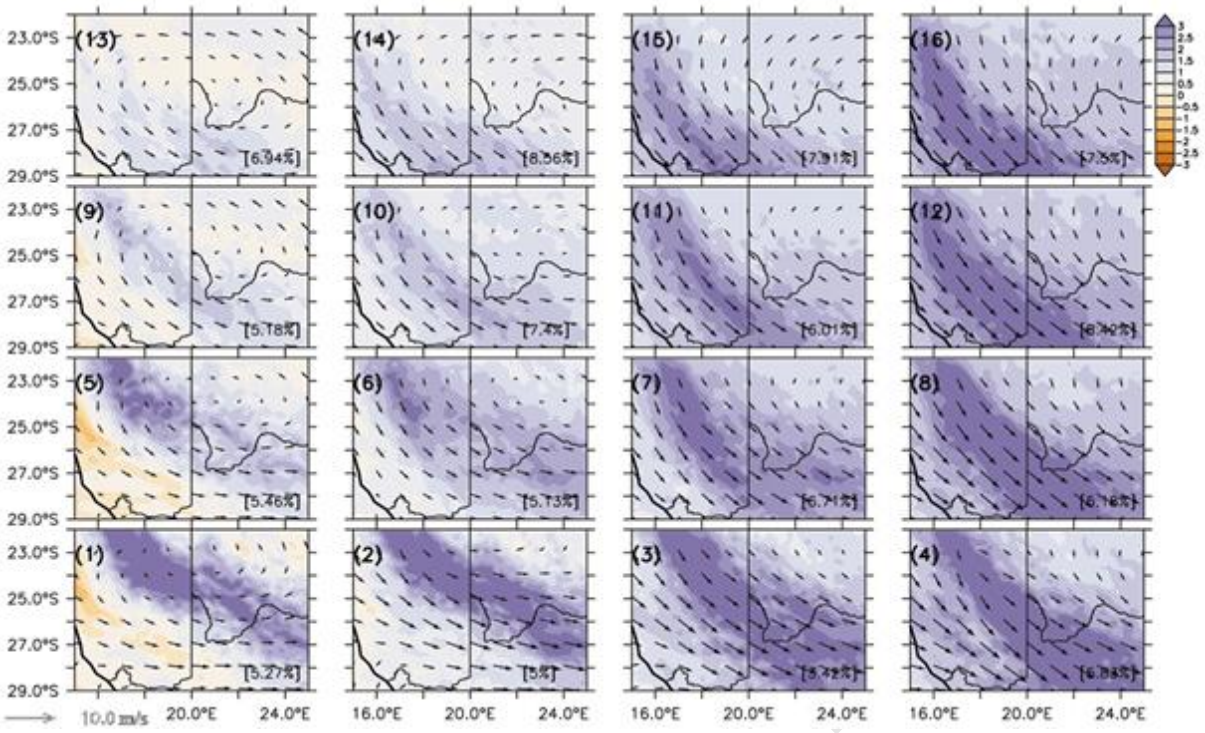

Figure 5.9: The SOM array of 850 hPa vertical wind (cm/s) in Autumn (MAM) over MWZ1 zone. Each node represents a synoptic vertical wind pattern over the MWZ1 zone. Negative value indicates downward motion and positive value indicates upward motion. The associated horizontal wind flows (m/s) at 850 hPa are indicated with arrows.

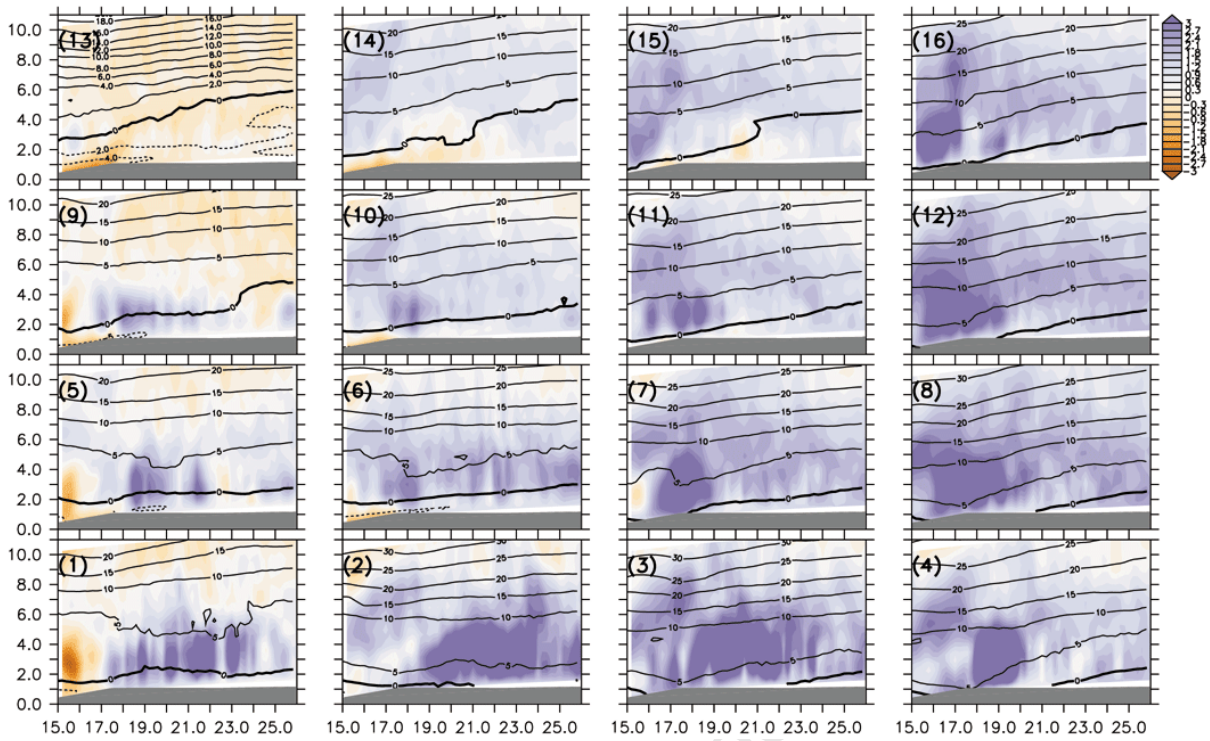

Figure 5.10: The corresponding vertical cross-section of vertical velocity (cm/s; colour) and zonal wind (m/s; contour) for the SOM array shown in Figure 5.9. The values are obtained at latitude 25^{o}S. The topography is indicated in grey. In vertical velocity, negative value indicates downward motion and positive value indicates upward motion. In the zonal wind, negative value (i.e. dashed contour) indicates easterly flow and positive value indicate westerly flow.

In JJA (Figure 5.11), all the SOM nodes can be considered as wave nodes, but with the different strength and pattern of vertical array motions. In Node (1), a strong upward motion with a north-west - south-east orientation is located at the centre of the domain and extends to the south-west corner with weak values, leaving the north-east corner for a weak downward motion. The entire domain is dominated by a north-westerly flow. In Node (13), the upward motion and downward motion cover almost equal areas of the domain; the upward motion covers the south-western half while the downward motion covers the north-eastern half. A strong north-westerly flow covers the area occupied by the upward motion, while a weak north-westerly flow covers the region occupied by the downward motion.

In Node (4), the upwards motion occupies the north-eastern half of the domain, while a weak downward motion dominates the south-western half of the domain. The area occupied by the vertical motion is dominated by north-westerly flow, while the area occupied by the weak downward motion is occupied by southerly flow. In Node (16), the upward motion is virtually pushed out of the domain; the weak upward motion is restricted to a small area in the north-eastern corner. Downward motion with southerly flow occupies the larger portion of the domain. The remaining nodes in this SOM array show a smooth transition among Nodes (1), (4), (13), and (16). The vertical cross-section (Figure 5.12) shows that a low-level westerly flow produces upward motion as it climbs the plateau, while a low-level easterly flow produces a downward motion as it descends the slope of the plateau.

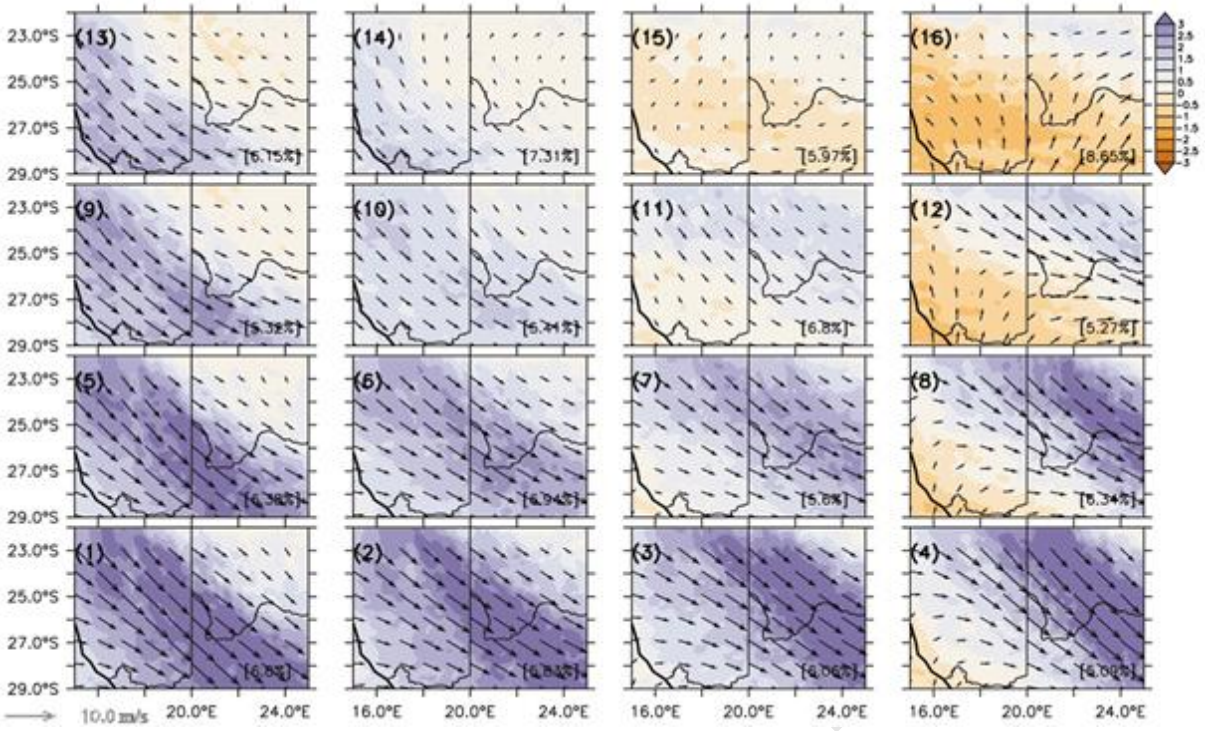

Figure 5.11: The SOM array of 850 hPa vertical wind (cm/s) in Winter (JJA) over MWZ1 zone. Each node represents a synoptic vertical wind pattern over the MWZ1 zone. Negative value indicates downward motion and positive value indicates upward motion. The associated horizontal wind flows (m/s) at 850 hPa are indicated with arrows.

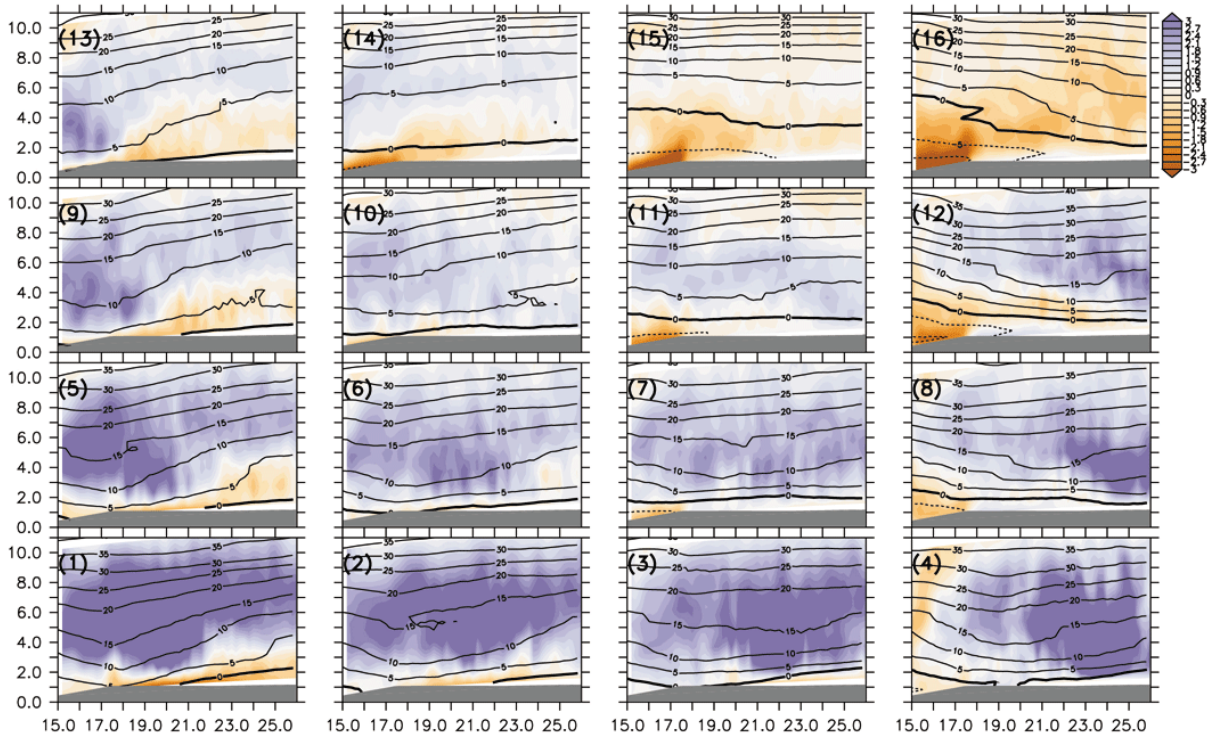

Figure 5.12: The corresponding vertical cross-section of vertical velocity (cm/s; colour) and zonal wind (m/s; contour) for the SOM array shown in Figure 5.11. The values are obtained at latitude 25°S. The topography is indicated in grey. In vertical velocity, negative value indicates downward motion and positive value indicates upward motion. In the zonal wind, negative value (i.e. dashed contour) indicates easterly flow and positive value indicate westerly flow.

In Spring (SON), Figure 5.13, the SOM array presents four wave nodes [Nodes (1), (2), (5),(6)]which typify 26% of the dataset. The wave nodes feature south-easterly winds (at the southern part of the domain) turning to westerly winds (at the northern part of the domain). The region with southern flow is associated with weak subsidence motion while the region with westerly flow is associated with upward motion. This is consistent with the results in other seasons. The non-wave nodes feature upward motion over the domain. The strength of the vertical motion and the location of the maximum strength vary with the nodes. Downward motion is present in the south west corner of MWZ1, while uplift is present to the north-east. The vertical cross-section, which shows the depth of the vertical wind, indicates that subsidence motion occurs where the easterly winds descend the Groot Karas Mountain range (Figure 5.14).

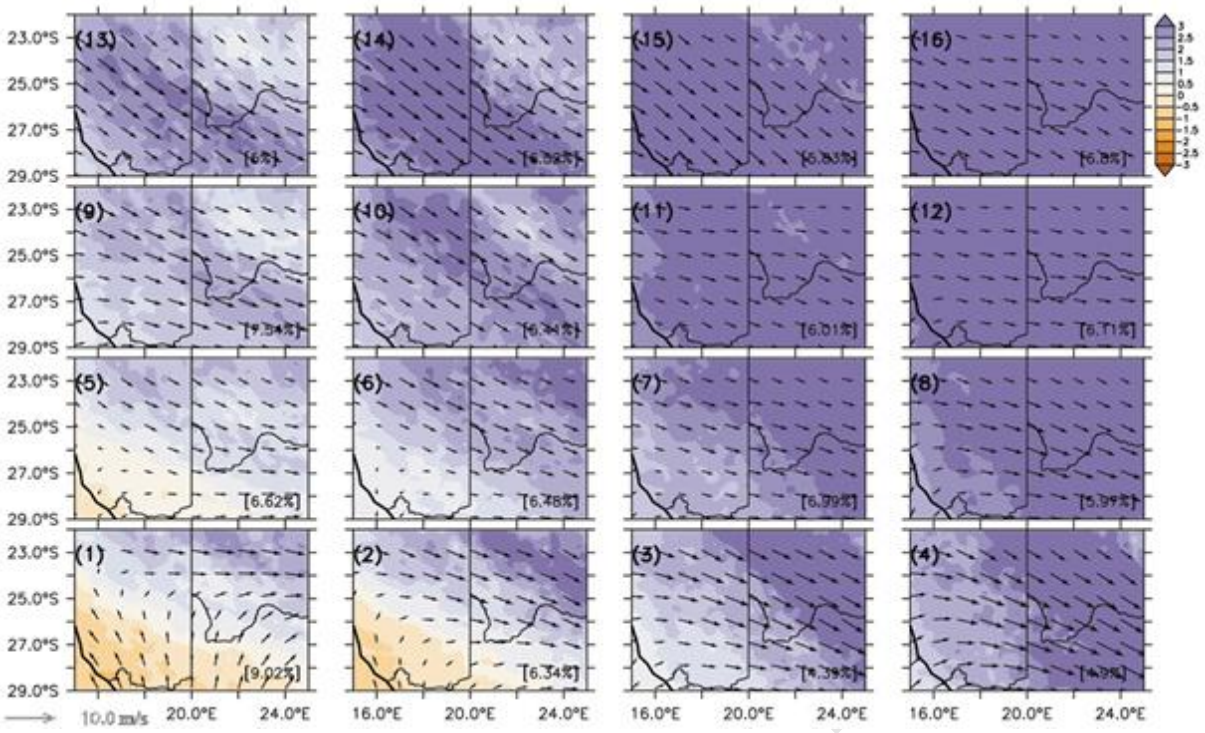

Figure 5.13: The SOM array of 850 hPa vertical wind (cm/s) in Spring (SON) over MWZ1 zone. Each node represents a synoptic vertical wind pattern over the MWZ1 zone. Negative value indicates downward motion and positive value indicates upward motion. The associated horizontal wind flows (m/s) at 850 hPa are indicated with arrows.

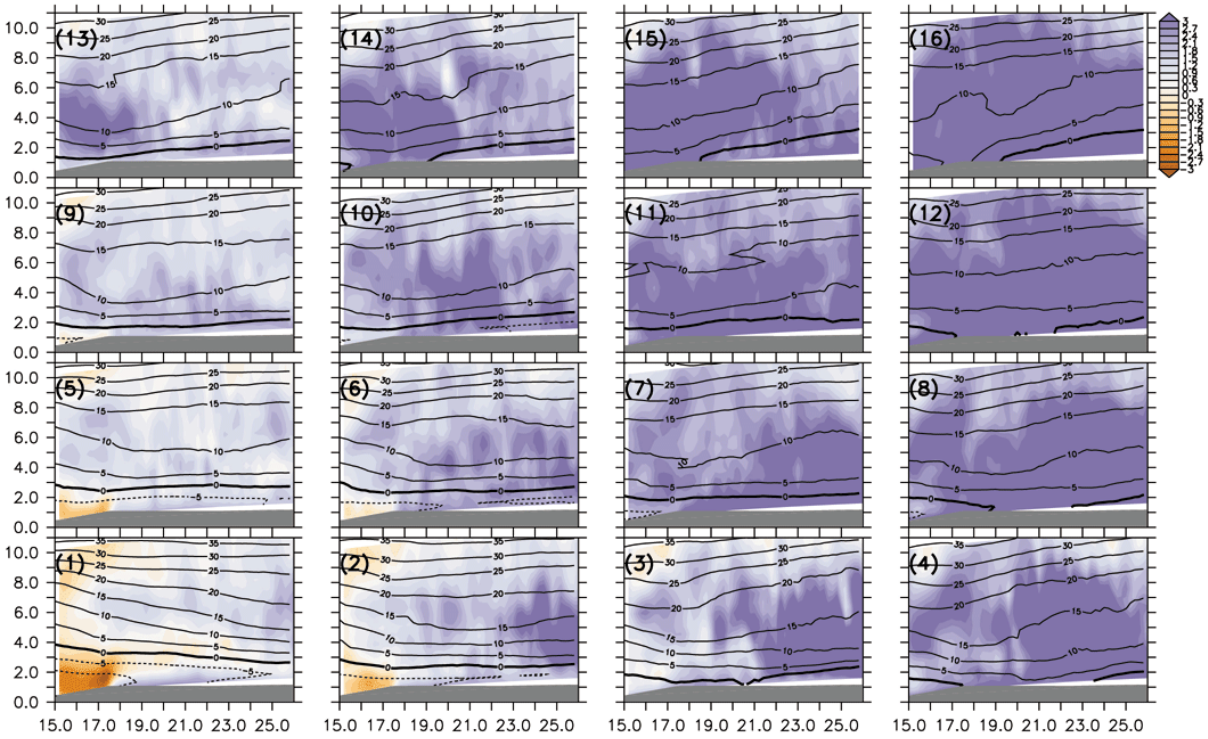

Figure 5.14: The corresponding vertical cross-section of vertical velocity (cm/s; colour) and zonal wind (m/s; contour) for the SOM array shown in Figure 5.13. The values are obtained at latitude 25°S. The topography is indicated in grey. In vertical velocity, negative value indicates downward motion and positive value indicates upward motion. In the zonal wind, negative value (i.e. dashed contour) indicates easterly flow and positive value indicate westerly flow.

With MWZ2, which covers south-eastern South Africa and the area off the coast, the SOM analysis shows different patterns of vertical motion and the patterns vary with seasons. In summer (DJF; Figure 5.15), the nodes are dominated by subsidence motion. Node (16) features an upward motion over the continent and subsidence over the ocean, and the domain is dominated by a westerly flow. Figure 5.16suggests that upward motion is induced by orographic lifting of the westerly flow over the Drakensberg range. However, the reverse is the case in Node (13), where a downward motion occurs over the Drakensberg range and upward motion occurs over the ocean. The upward motion could be induced by the warm ocean current heating, but the upward motion is shallower than that seemingly induced by the orographic lifting. The non-wave nodes show only subsidence motion, with peak focuses between areas to the south-east, Node (1), the south, Node (5), and the east, Node (4). There is only weak subsidence focused over the continent.

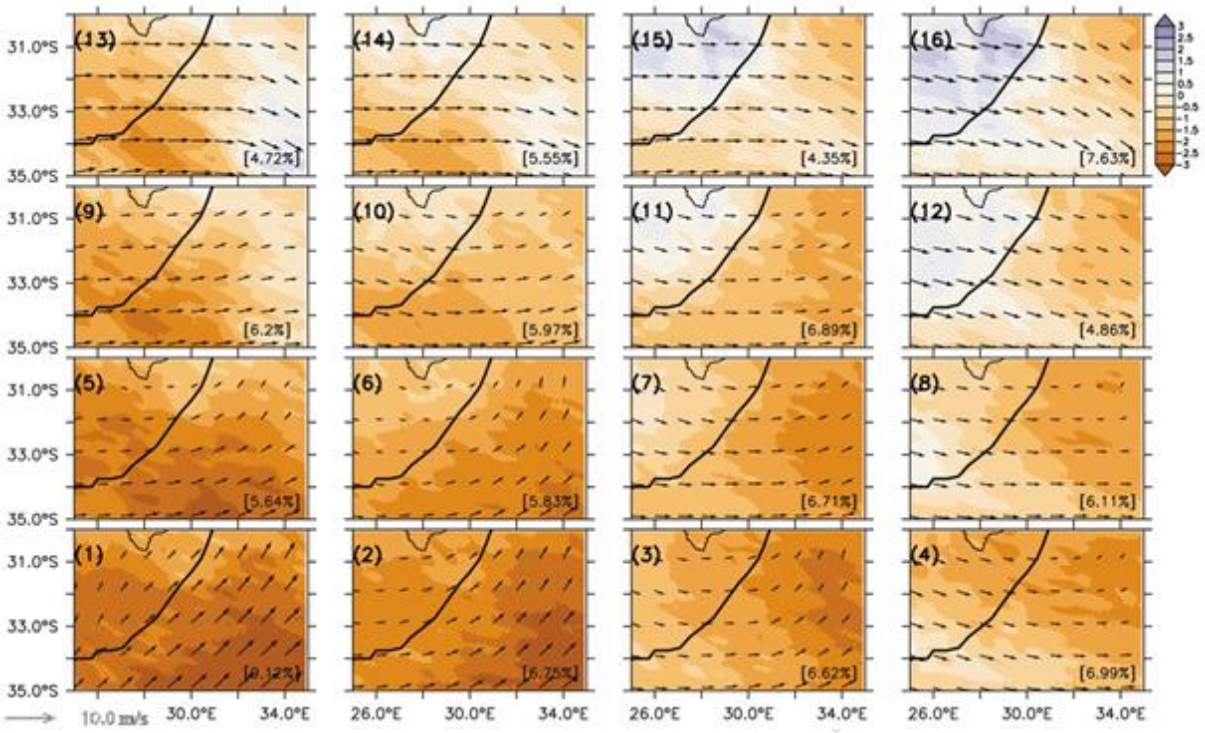

Figure 5.15: The SOM array of 850 hPa vertical wind (cm/s) in Summer (DJF) over MWZ2 zone. Each node represents a synoptic vertical wind pattern over the MWZ2 zone. Negative value indicates downward motion and positive value indicates upward motion. The associated horizontal wind flows (m/s) at 850 hPa are indicated with arrows.

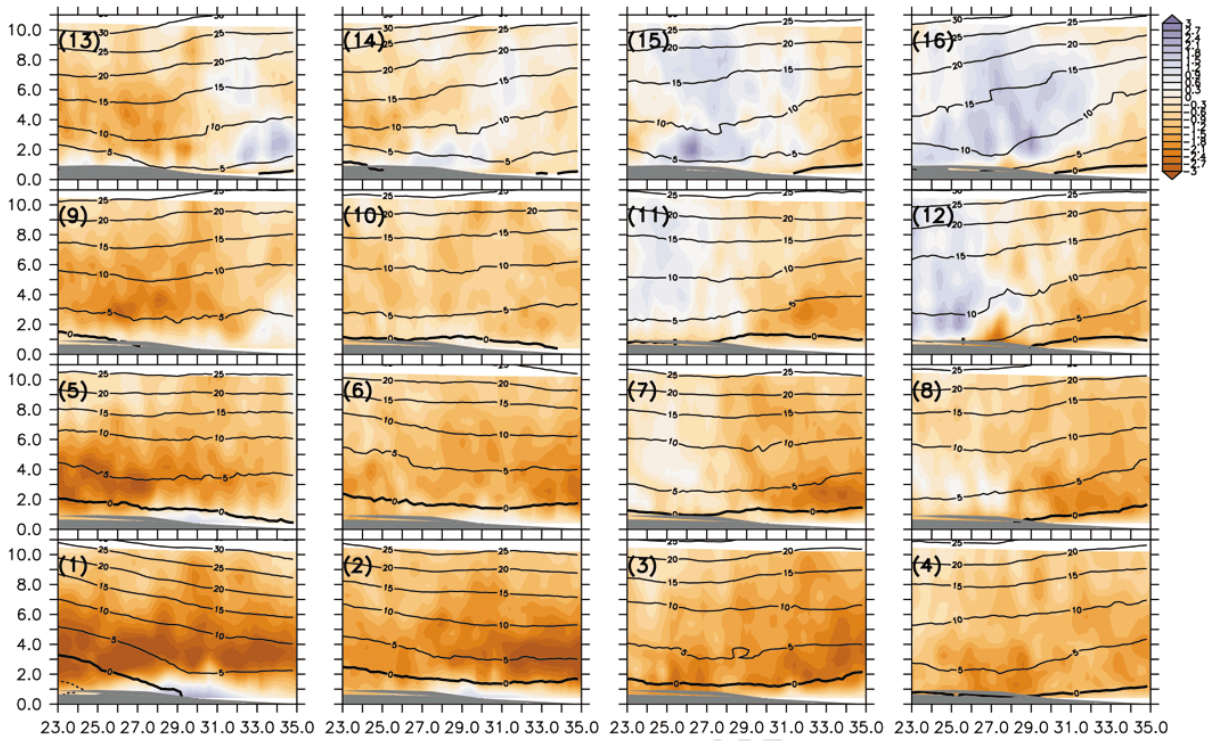

Figure 5.16: The corresponding vertical cross-section of vertical velocity (cm/s; colour) and zonal wind (m/s; contour) for the SOM array shown in Figure 5.15. The values are obtained at latitude 33^{o}S. The topography is indicated in grey. In vertical velocity, negative value indicates downward motion and positive value indicates upward motion. In the zonal wind, negative value (i.e. dashed contour) indicates easterly flow and positive value indicate westerly flow.

Wave nodes in MAM (Figure 5.17) are represented by two types of nodes. Nodes (1,2,3,7,8), 33% occurrence, show weak surface easterlies undercutting the westerly wind from the continental plateau and inducing an elevation of upward motion away from the Drakensberg range (Figure 5.18). On the other hand, nodes (12,14,15,16 – 15%), in the presence of strong westerly surface winds, follow the dramatic decrease in elevation, as the topography flattens and therefore shows as downward motion. The strong westerly flow however reduces the likelihood of the wave merging back into the flow, and this oscillation appears to duct away from the topography. The remaining non-wave nodes show a majority of air with upward motion, with the exception of node (4) in which air is sinking and the horizontal wind gains a more southerly component.

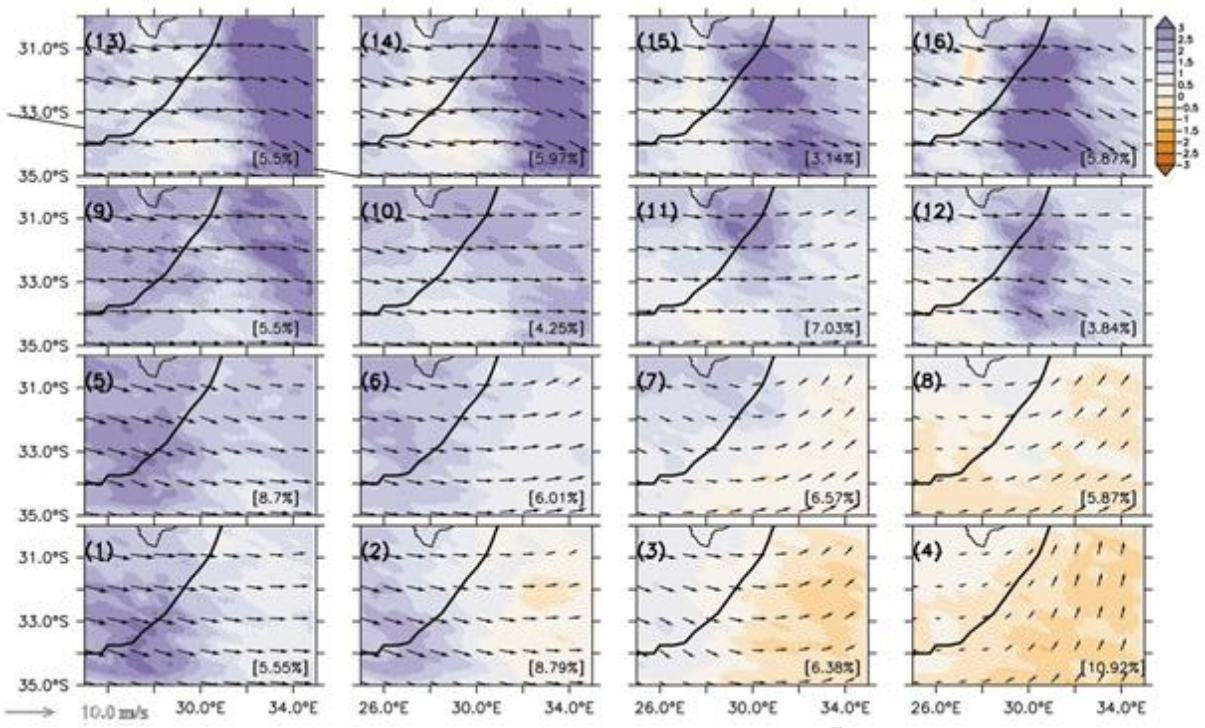

Figure 5.17: The SOM array of 850 hPa vertical wind (cm/s) in Autumn (MAM) over MWZ2 zone. Each node represents a synoptic vertical wind pattern over the MWZ2 zone. Negative value indicates downward motion and positive value indicates upward motion. The associated horizontal wind flows (m/s) at 850 hPa are indicated with arrows.

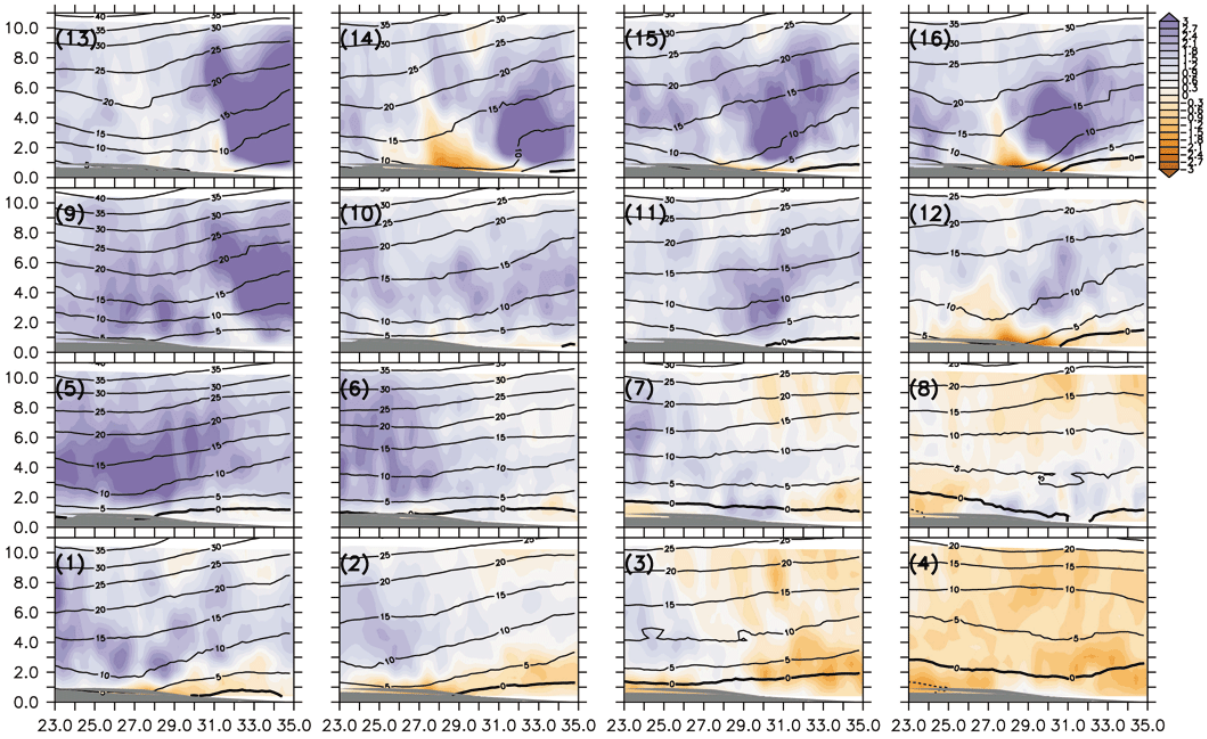

Figure 5.18: The corresponding vertical cross-section of vertical velocity (cm/s; colour) and zonal wind (m/s; contour) for the SOM array shown in Figure 5.17. The values are obtained at latitude 33^{o}S. The topography is indicated in grey. In vertical velocity, negative value indicates downward motion and positive value indicates upward motion. In the zonal wind, negative value (i.e. dashed contour) indicates easterly flow and positive value indicate westerly flow.

JJA SOM nodes present varied vertical wind activity in Figure 5.19. JJA has seven wave nodes (2), (9), (10), (13), (14), (15), (16) accounting for 35% occurrence. With the exception of node (2) which has upward motion over the continent and sinking air over the ocean, there is downward motion on the western side of the domain over the continent and upward motion to the west in these nodes. The cross-section of these nodes shows a domination of westerly winds in the region (Figure 5.20). These winds appear to sink as they descend the Drakensberg range at 28°E. This wave propagates to the east where upward motion occurs and the wave rejoins with the dominating zonal wind flow. The remaining non-wave nodes are dominated by either upward motion [nodes (1), (5), (6) – 19 % occurrence] or by downward motion [nodes (3), (4), (7), (8), (11), (12) – 45 % occurrence].

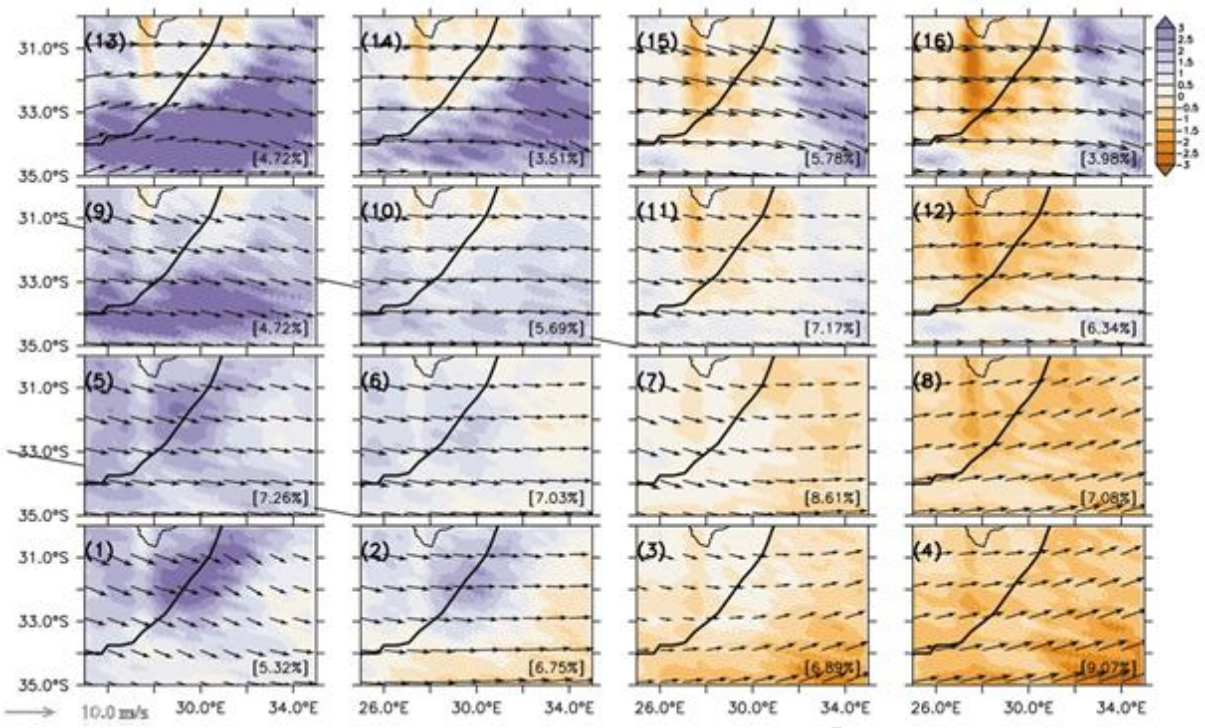

Figure 5.19: The SOM array of 850 hPa vertical wind (cm/s) in Winter (JJA) over MWZ2 zone. Each node represents a synoptic vertical wind pattern over the MWZ2 zone. Negative value indicates downward motion and positive value indicates upward motion. The associated horizontal wind flows (m/s) at 850 hPa are indicated with arrows.

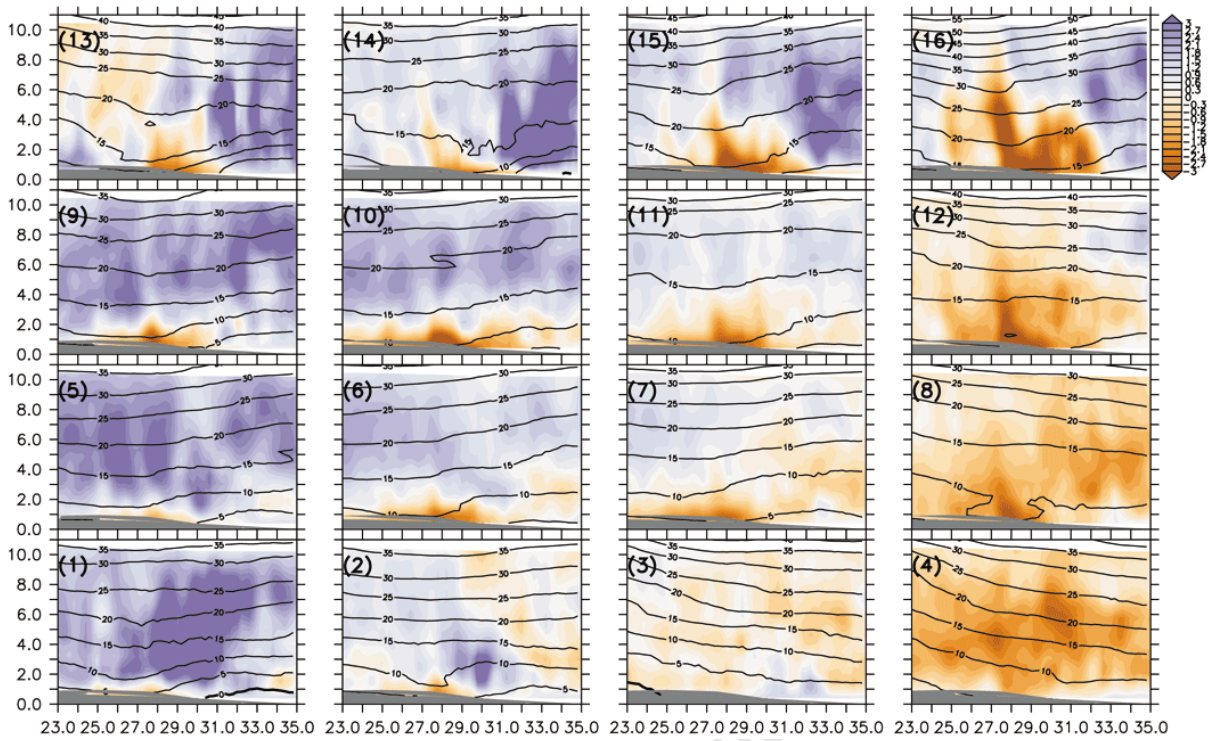

Figure 5.20: The corresponding vertical cross-section of vertical velocity (cm/s; colour) and zonal wind (m/s; contour) for the SOM array shown in Figure 5.19. The values are obtained at latitude 33^{o}S. The topography is indicated in grey. In vertical velocity, negative value indicates downward motion and positive value indicates upward motion. In the zonal wind, negative value (i.e. dashed contour) indicates easterly flow and positive value indicate westerly flow.

The SOM nodes in SON show a majority of upward moving air in MWZ2 with some exceptions (Figure 5.21). Nodes (1), (2), (5) show a majority of descending air. Wave nodes (3), (4) show upward motion in the southern part of the domain and downward motion over the continent (11% occurrence). Nodes (9), (13) present descending motion at 28°E associated with movement down the Drakensberg range (9% occurrence). The cross-section (Figure 5.22) shows several nodes [(1), (2), (3), (4), (5), (9), (13)] with descending motion at 28°E. These nodes all have strong surface westerly winds and therefore show enhanced downward motion as they descend the Drakensberg range. All the remaining nodes have a decreased surface wind speed and therefore do not exhibit strong downward motion at 28°E.

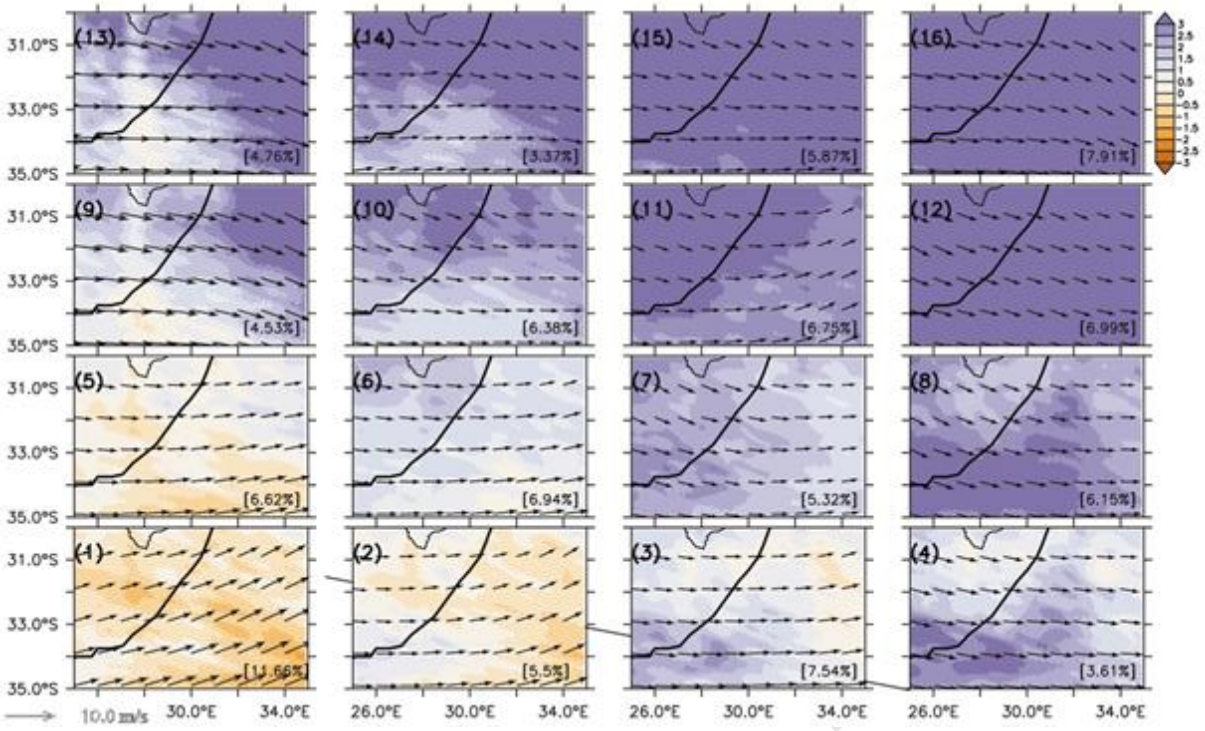

Figure 5.21: The SOM array of 850 hPa vertical wind (cm/s) in Spring (SON) over MWZ2 zone. Each node represents a synoptic vertical wind pattern over the MWZ2 zone. Negative value indicates downward motion and positive value indicates upward motion. The associated horizontal wind flows (m/s) at 850 hPa are indicated with arrows.

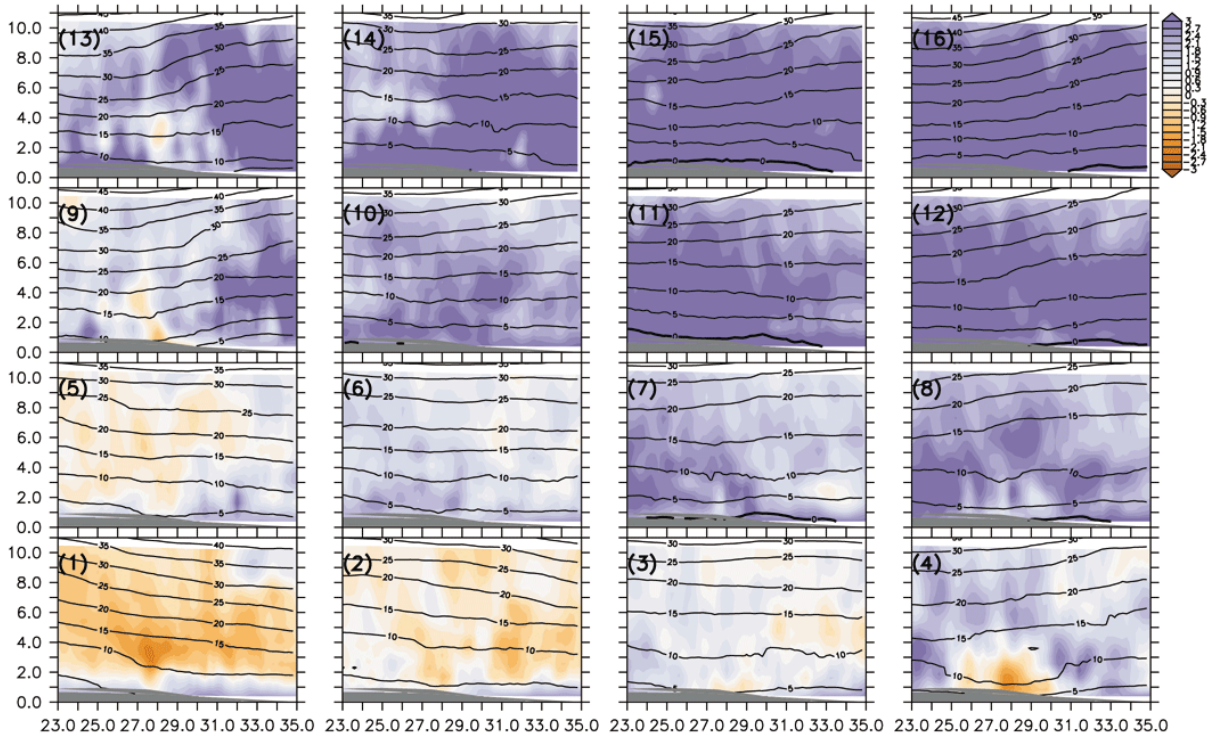

Figure 5.22: The corresponding vertical cross-section of vertical velocity (cm/s; colour) and zonal wind (m/s; contour) for the SOM array shown in Figure 5.21. The values are obtained at latitude 33^{o}S. The topography is indicated in grey. In vertical velocity, negative value indicates downward motion and positive value indicates upward motion. In the zonal wind, negative value (i.e. dashed contour) indicates easterly flow and positive value indicate westerly flow.

Chapter 6. Conclusion

This work studies, for the first time, the intensity and seasonal distribution of inertia gravity wave activity over Southern Africa using a high resolution dataset. Owing to the dearth of high spatial and temporal resolution observational data in this area, the work used a modelling approach to do the study. To overcome the limitations of GCMs resolution in resolving meso-scale features, and the boundary condition errors in RCM simulations, the study used a GCM with capability for grid stretching to simulated global climate features but with a high resolution (10 km) over Southern Africa. The hourly data from the simulation were analysed for the study.

Validation was undertaken for the simulated surface temperature, precipitation and wind, and vertical velocity fields against the NCEP reanalysis data. The results showed that the model gives a realistic simulation of the climatological features over the globe and specifically over Southern Africa. However, there are some inconsistencies between simulated model and observational fields, particularly on the Southern African scale. But the dynamics of the simulated features agree well with observation, and they present realistic seasonal changes in the fields between January and June through the seasonal cycle.

Variance analysis was used to identify regions of consistent vertical wind variability that acts as an indication of wave activity. The analysis indentified two main zones with wave activity, namely: southern Namibia (to the east of the Groot Karas Mountains) and south-east of South Africa (the east of the Drakensberg). The third zone (MWZ3) is over the Western Cape of South Africa (along the Cape Fold Belt) and is not discussed in depth, as the activity is present only during the winter and spring seasons.

Fourier analysis was used to study the power spectrum of wave activities in the two major zones. The analysis shows that the wave activities seem to follow the power law, showing the transfer through wind mixing of energy from long inertial waves to short inertial waves.SOM analysis grouped vertical wind states in the hotspot zones by common characteristics. SOMs also presented the occurrence of each node to give an indication of the spatial distribution and frequency of wave activity.

The circulation and the vertical atmospheric profiles are shown for the dominating wave nodes to give an indication of the vertical penetration of the dominating wave activity. The orientation of differing wave excitation nodes revealed in the SOMs of summer and autumn tend to be north-west to south-east in the southern Namibian zone, Additionally, these months exhibit peaks in the 8 – 10-hour period and a strong wave peak at the 24-hour period indicating orographic, convective and diurnal cycle wave excitement. Both winter and spring months present broader variations in wave activity and also do not show the shorter period wave activity peak, but only the diurnal one. This seems to be because, in DJF, the diurnal signal is persistent and strong and therefore dulls out a shorter signal and in JJA, there are minimal convective activity and therefore no short frequency wave strength present in the vertical wind. While the diurnal cycle does present an influence on the vertical wave activity, strong horizontal winds interacting with topography and the convective tropical temperate trough development in spring appear to be the primary source of wave excitation during these months in MWZ1.

In MWZ2, to the east of the Drakensberg, the convectively dominated summer months are evidenced through the location of rising air over land and the peaks in wave activity at 8 -10 hours and 24 hours respectively. Autumn and spring share a similar excitation regime of strong horizontal wind speed inducing increased wave activity when striking the Drakensberg, also expressed by a majority of strong wave activity focused off-shore and the dearth of convective peaks in the wave spectrum, with the exception of the diurnal cycle. The winter months express no such short wavelength peaks but rather exhibit a longer wavelength, theoretically induced by orographic interaction.

The horizontal SOMs illustrated the seasonal distribution and frequency of wave occurrence in each of the zones, while the vertical cross-sections were a power-tool for presenting the structure of the troposphere responsible for the wave activity. These tools suggested that while convective activity was often responsible for the general upward motion, orographic forcing resulted in a significant propagating wave activity.

In MWZ1, easterlies seemed often to result in air sinking down the Groot Karas Mountain range presenting wave activity higher in the atmosphere; alternatively surface westerlies are assumed to rise, forced over the orographic barrier. General convective upward motion is however present throughout. MWZ2 was dominated by westerly wind, which probably resulted in orographic uplift inducing wave activity. When the surface wind was strong (particularly in JJA), it travelled down the face of the Drakensberg and induced downward motion.

These findings of seasonal variation of wave intensity and location bear similarity to studies conducted previously over South Africa. Alexander et al. (2008) presents minimum large-scale wave activity during summer. As Namboothiri et al. (2008) suggests, there is rather a dominance of only convectively generated waves. The high wave activity zone of southern Namibia is present in autumn (Alexander et al., 2008).Although wave activity is more intense and larger in autumn, wave activity is reduced in spring and winter (Zhang et al., 2012).Large-scale inertial gravity wave activity peaks over the region during winter, particularly to the south (Zhang et al., 2012). Minimum convective influence is present, even on the diurnal scale (Namboothiri et al., 2008), and wave activity is located downwind of large orographic barriers, in line with observations from Eckermann and Wu (2012). Of note is activity to the east of the Drakensberg range.

Austral spring shows a similar wave distribution to autumn, but with greater intensity and coverage, particularly in the southern Namibian region (Alexander et al., 2008), theoretically influenced by the TTT system. These months exhibit wave strength second only to the winter months (Zhang et al., 2012)

The model simulation and the analysis thereof seemingly showed that interaction between horizontal wind and orographic features is an important cause of inertial gravity wave excitation over Southern Africa. Additionally convection also accounts for some wave activity in the warmer months. These waves have increased strength at the longer periods and wavelengths, particularly in winter, but exhibit discernible peaks between the seasons based on influences such as convective activity and diurnal cycles in the summer months.

This work does make some assumptions and is therefore limited in its application. One such assumption is that variance in the vertical wind field can be utilised to suggest the presence of atmospheric wave activity, and therefore areas of high and persistent variance are the most active wave zones in the domain. These assumptions lead to the identification of the two primary waves zones that were analyzed further. It also suggests that the primary excitation mechanism of this activity wave is topographical interference with horizontal wind fields and convective uplift. Neither of these assumptions were explicitly tested but rather suggested as plausible causes of wave activity.

This work also suffers from the limited duration of the analyzed simulation; potential work following on from this study should consist of multi-year model simulations. This would provide a more robust climatological analysis by accounting for inter-annual variability in spatial, temporal and intensity terms. The results are also model specific. The study would therefore benefit from a multi-model ensemble. Additionally, studying the synoptic conditions in the seasons exhibiting the strongest wave activity would add substantial backup to the suggested wave excitation mechanisms. Longer simulations would present information on decadal variability and the influence of large-scale circulations, like MJO or ENSO, may have on inertia gravity wave if model initial states are forced by observation. Given the contribution vertical waves have on atmospheric momentum and mixing, it would also be invaluable to simulate the inertial gravity wave response to climate change by analysing wave output after initialising the model with an IPCC SRES scenario.

Chapter 7. Bibliography

Abiodun, B. J., Prusa, J. M., and Gutowski, W. J. (2008).Implementation of a non-hydrostatic, adaptive-grid dynamics core in CAM3. Part I: comparison of dynamics cores in aqua-planet simulations. *Climate Dynamics*, (31), 795-810. doi: 10.1007/s00382-008-0381-y.

Alexander, S. P., Tsuda, T., Kawatani, Y., and Takahashi, M. (2008). Global distribution of atmospheric waves in the equatorial upper troposphere and lower stratosphere : COSMIC observations of wave mean flow interactions. *Journal of Geophysical Research*, *113*, 1-18. doi: 10.1029/2008JD010039.

Allen, S. J, and Vincent, R. A. (2005). Gravity wave activity in the lower atmosphere: Seasonal and latitudinal variations. *Journal of Geophysical Research*, *100*(May), 1327-1350.

Ambrizzi, T. and Hoskins, B. J. (1997).Stationary rossby-wave propagation in a baroclinic atmosphere. *Quarterly Journal of the Royal Meteorological Society*, *123*(540), 919-928.

Ambroisea, C., Sèzeb, G., Badranc, F. and Thiriad, S. (2000).Hierarchical clustering of self-organizing maps for cloud classification. *Neurocomputing*, *30*(1-4), 47-52.

Azzali, S., and Menenti, M. (1999).Mapping vegetation-soil-climate complexes in southern Africa using temporal Fourier analysis of NOAA-AVHRR NDVI data. *International Journal of Remote Sensing*, *21*(21), 37-41.

Bain, C. L., Parker, D. J., Dixon, N., Fink, A. H., Taylor, C. M., Brooks, B., et al. (2011).Anatomy of an observed African easterly wave in July 2006.*Quarterly Journal of the Royal Meteorological Society*, *137*(April 2011), 923-933. doi: 10.1002/qj.812.

Baumgaertner, A. J. and Mcdonald, A. J. (2007). A gravity wave climatology for Antarctica compiled from Challenging Minisatellite Payload / Global Positioning System (CHAMP / GPS) radio occultations. *Journal of Geophysical Research*, *112*, 1-12. doi: 10.1029/2006JD007504.

Beguin, O., Martius, O., Sprenger, M., Spichtinger, P., Folini, D., Wernli, H., et al. (2012). Short Communication Tropopause level Rossby wave breaking in the Northern Hemisphere : a feature-based validation of the ECHAM5-HAM climate model. *International Journal of Climatology*.doi: 10.1002/joc.3631.

Bretherton, F. P. (1966). The propagation of groups of internal gravity waves in a shear flow. *Quarterly Journal of the Royal Meteorological Society*, *92*(394), 466-480.

Burpee, R. W. (1972).The origin and structure of Easterly Waves in the Lower Troposphere of North Africa. *Journal of the Atmospheric Sciences*, *29*, 77-90.

Cahn, A. (1945). An investigation of the free oscillations of a simple current system. *Journal of Meteorology*, *2*, 113-119.

Chandran, A., Collins, R. L., Garcia, R. R. and Marsh, D. R. (2011). A case study of an elevated stratopause generated in the Whole Atmosphere Community Climate Model. *Geophysical Research Letters*, *38*(December 2010), 1-6. doi: 10.1029/2010GL046566.

Chang, L. C., Liu, J. and Palo, S. E. (2011).Propagating planetary wave coupling in SABER MLT temperatures and GPS TEC during the 2005/2006 austral summer. *Journal of Geophysical Research: Space Physics (1978–2012)*, *116*(A10).

Charney, J. G., and Drazin, P. G. (1961).Propagation of planetary-scale disturbances from the lower into the upper atmosphere. *Journal of Geophysical Research*, *66*, 83-109.

Clarka, R., Burrageb, M., Frankec, S., Mansond, A., Meekd, C., Mitchelle, N., et al. (2002).Observations of 7-d planetary waves with MLT radars and the UARS-HRDI instrument. *Journal of Atmospheric and Solar-Terrestrial Physics*, *64*(8-11), 1217-1228.

Cogley, J. G. (1991).GGHYDRO–Global Hydrographic Data Release 2.0.*Trent Climate Note*, *91*(1).

Collins, W. D., Bitz, C. M., Blackmon, M. L., Bonan, G. B., Bretherton, C. S., Carton, J. A., et al. (2006). The Community Climate System Model Version 3 (CCSM3).*journal of Climate*, *19*, 2122-2143.

Collins, W. D., Rasch, P. J., Boville, B. A., Hack, J. J., McCaa, J. R., Williamson, D. L., et al. (2004). *Description of the NCAR Community Atmosphere Model (CAM 3.0)*. Boulder, Colorado: National Center For Atmospheric Research.

Crane, R. G., and Hewitson, B. C. (1998).Doubled CO2 precipitation changes for the Susquehanna Basin: down-scaling from the Genesis general circulation model. *International Journal of Climatology*, *18*(1), 65-76.

Cretat, J., Pohl, B., Richard, Y. and Drobinski, P. (2012). Uncertainties in simulating regional climate of Southern Africa : sensitivity to physical parameterizations using WRF. *Climate Dynamics*, *38*, 613-634. doi: 10.1007/s00382-011-1055-8.

Dalin, P., Kirkwood, S., Hervig, M., Mihalikova, M., Mikhaylova, D., Wolf, I., et al. (2012). Wave influence on polar mesosphere summer echoes above Wasa : experimental and model studies. *Annales Geophysicae*, *30*, 1143-1157. doi: 10.5194/angeo-30-1143-2012.

Domeisen, D. I., and Plumb, R. A. (2012). Traveling planetary-scale Rossby waves in the winter stratosphere : The role of tropospheric baroclinic instability. *Geophysical Research Letters*, *39*(October), 1-5. doi: 10.1029/2012GL053684.

Dube, L. T. (2012). Climate of Southern Africa. *Routledge*.

Eckermann, S. D. and Wu, D. L. (2012).Satellite detection of orographic gravity-wave activity in the winter subtropical stratosphere over Australia and Africa. *Geophysical Research Letters*, *39*(October), 1-6. doi: 10.1029/2012GL053791.

Ellrod, G. P. (1991). An objective clear-air turbulence forecasting technique: verification and operational use. *Weather and Forecasting*, *7*, 150-165.

Finnis, J., Cassano, J., Holland, M., Serreze, M. and Uotila, P. (2009). Synoptically forced hydroclimatology of major Arctic watersheds in general circulation models; Part 1: the Mackenzie River Basin. *International Journal of Climatology*, *29*(9), 1226-1243.

Freitas, A. C., Rao, V. B. (2011).Multidecadel and interannual changes of stationary Rossby waves. *Quarterly Journal of the Royal Meteorological Society*, *137*, 2157-2173.

Fritts, D. C., and Alexander, M. J. (2003). *Gravity Wave Dynamics and Effects in the Middle Atmosphere* (pp. 1-124).

Fritts, D. C. and Rastogi, P. K. (1985). Convective and dynamical instabilities due to gravity wave motions in the lower and middle atmosphere: Theory and observations. *Radio Sci*, *20*, 1247-1277.

Gavrilov, N. M. and Fukao, S. (2001). Hydrodynamic tropospheric wave sources and their role in gravity wave climatology of the upper atmosphere from the MU radar observations. *Journal of Atmospheric and Solar-Terrestrial Physics*, *63*, 931-943.

Geisler, J. E. and Dickinson, R. E. (1972). The role of variable coriolis parameter in the propagation of inertia-gravity waves during the process of geostrophic adjustment. *Journal of Physical Oceanography*, *2*, 263-272.

Geller, M. A., Liu, H., Richter, J. H., Wu, D., and Zhang, F. (2006). Gravity Waves in Weather , Climate , and Atmospheric Chemistry : Issues and Challenges for the Community. *Atmospheric Research*.

Grimsdell, A. W., Alexander, M. J., May, P. T. and Hoffmann, L. (2010). Model study of waves generated by convection with direct validation by satellite. *Journal of the atmospheric Sciences*, *67*, 1617-1631.

Hardiman, S. C., Butchart, N., Osprey, S. M., Gray, L. J., Bushell, A. C., Hinton, T. J., et al. (2010). The Climatology of the Middle Atmosphere in a Vertically Extended Version of the Met Office ' s Climate Model . Part I : Mean State. *Journal of the atmospheric Sciences*, *67*, 1509-1525.doi: 10.1175/2009JAS3337.1.

Hemer, M. A., Church, J. A., and Hunter, J. R. (2010).Variability and trends in the directional wave climate of the Southern Hemisphere. *International Journal of Climatology*, *30*(4), 475-491.

Hewitson, B. C., and Crane, R. G. (2002). Self-organizing maps : applications to synoptic climatology. *Climate Research*, *22*, 13-26.

Hines, C. O. (1960). Internal Atmospheric Gravity Waves at Ionspheric Heights. *Canadian Journal of Physics*, *38*(11), 60-150.

Hines, C. O. (1971). Generalizations of the Richardson criterion for the onset of atmospheric turbulence. *Quarterly Journal of the Royal Meteorological Society*, *97*(414), 429-439.

Hocking, W. K., and Kumar, K. G. (2011).Long term behavior of the MLT quasi-7-day wave at two radar-sites at northern polar latitudes. *Journal of Atmospheric and Solar-Terrestrial Physics*, *73*, 1616-1628. doi: 10.1016/j.jastp.2011.02.004.

Hodges, R. R. (1967). Generation of turbulence in the upper atmosphere by internal gravity waves. *Journal of Geophysical Research*, *72*(13), 3455-3458.

Janney, P. E., Shirey, S. B., Carlson, R. W., Pearson, D. G., Bell, D. R., Roex, A. P., et al. (2010). Age , Composition and Thermal Characteristics of South African Off-Craton Mantle Lithosphere : Evidence for a Multi-Stage History. *Journal of Petrology*, *51*(9), 1849-1890. doi: 10.1093/petrology/egq041.

Jayaraman, A., Ratnam, M. V., Patra, A. K., Rao, T. N., Sridharan, S., Rajeevan, M., et al. (2010). Study of Atmospheric Forcing and Responses (SAFAR) campaign : overview. *Annales Geophysicae*, *28*, 89-101.

Kohonen, T. (1982).Self-organized formation of topologically correct feature maps. *Biological Cybernetics*, *43*(1), 59-69.

Kohonen, T. (2001).*Self-Organizing Maps*.(T. S. Huang and M. R. Schroeder) (3rd.).Springer.

Kuester, M. A., Alexander, M. J. and Ray, E. A. (2008). A Model Study of Gravity Waves over Hurricane Humberto(2001). *Journal of the Atmospheric Science*, *65*(2001), 3231-3246. doi: 10.1175/2008JAS2372.1.

Lindzen, R. S. (1981). Turbulence and stress owing to gravity wave and tidal breakdown. *Journal of Geophysical Research*, *86*, 9707-9714.

Llamedo, P., de La Torre, A., Alexander, P., Luna, D., Schmidt, T., Wickert, J., et al. (2009). A gravity wave analysis near to the Andes Range from GPS radio occultation data and mesoscale numerical simulations : Two case studies. *Advances in Space Research*, *44*, 494-500. doi: 10.1016/j.asr.2009.04.023.

Magalhaes, J. M., Araujo, I. B., da Silva, J. C., Grimshaw, R. H., Davis, K., Pineda, J., et al. (2011). Atmospheric gravity waves in the Red Sea : a new hotspot. *Nonlinear Processes in Geophysics*, 71-79. doi: 10.5194/npg-18-71-2011.

Malmgren, B. R., and Winter, A. (1998). Climate Zonation in Puerto Rico Based on Principal Components Analysis and an Artificial Neural Network. *journal of Climate*, *12*.

Mason, S. J., and Jury, M. R. (1997). Climatic variability and change over southern Africa : a reflection on underlying processes. *Progress in Physical Geography*, *21*(1), 23-50. doi: 10.1177/030913339702100103.

Mied, R. P. (1976). The occurrence of parametric instabilities in finite-amplitude internal gravity waves. *Journal of Fluid Mechanics*, *78*(04), 763-794.

Monserrat, S., and J.A., T. (1996).Use of ducting theory in an observed case of gravity waves. *Journal of the Atmospheric Sciences*, *53*, 1724-1736.

Moore, A., Blenkinsop, T. and Cotterill, F. W. (2009). Southern African topography and erosion history : plumes or plate tectonics ? *Terra Nova*, *21*, 310-315. doi: 10.1111/j.1365-3121.2009.00887.x.

Namboothiri, S. P., Jiang, J. H., Kishore, P., Igarashi, K., Ao, C. O., Romans, L. J., et al. (2008). CHAMP observations of global gravity wave fields in the troposphere and stratosphere. *Journal of Geophysical Research*, *113*, 1-11. doi: 10.1029/2007JD008912.

Nappo, C. J. (2002). *An Introduction to atmospheric Gravity waves*.(R. Dmowska, J. R. Holton, and H. T. Rossby) (Volume 85.). Tennessee: International Geophysics Series.

Ndarana, T., and Waugh, D. W. (2010).The link between cut-off lows and Rossby wave breaking in the. *Quarterly Journal of the Royal Meteorological Society*, *136*(April), 869-885. doi: 10.1002/qj.627.

Newell, R. E. (1964). Stratospheric energetics and mass transport. *Pure and Applied Geophysics*, *58*(1), 145-156.

Newell, R. E., and Dickinson, R. E. (1967).On the application of a proposed global system for measuring meteor winds. *Pure and Applied Geophysics*, *68*(1), 162-172.

Nicolls, M. J. and Heinselman, C. J. (2007).Three-dimensional measurements of traveling ionospheric disturbances with the Poker Flat Incoherent Scatter Radar. *Geophysical Research Letters*, *34*(August), 1-6. doi: 10.1029/2007GL031506.

Nicolls, M. J., Varney, R. H., Vadas, S. L., Stamus, P. A., Heinselman, C. J., Cosgrove, R. B., et al. (2010). Influence of an inertia-gravity wave on mesospheric dynamics : A case study with the Poker Flat Incoherent Scatter Radar. *Journal of Geophysical Research*, *115*, 1-24. doi: 10.1029/2010JD014042.

O'Sullivan, D. and Dunkerton, T. J. (1995). Generation of inertia-gravity waves in a simulated life cycle of baroclinic instability. *Journal of the Atmospheric Science*, *52*, 3695-3716.

Pancheva, D. and Laštovička, J. (1998). Planetary wave activity in the lower ionosphere during CRISTA I campaign in autumn 1994 (October-November). *Annales Geophysicae*, *16*(8), 1014-1023.

Pearce, J. L., Beringer, J., Nicholls, N., Hyndman, R. J., Uotila, P., Tapper, N. J., et al. (2011). Investigating the influence of synoptic-scale meteorology on air quality using self-organizing maps and generalized additive modelling. *Atmospheric Environment*, *45*, 128-136. doi: 10.1016/j.atmosenv.2010.09.032.

Plougonven, R. and Snyder, C. (2005). Gravity waves excited by jets : Propagation versus generation. *Geophysical Research Letters*, *32*, 1-4. doi: 10.1029/2005GL023730.

Plougonven, R., Teitelbaum, H. and Zeitlin, V. (2003).Inertia gravity wave generation by the tropospheric midlatitude jet as given by the Fronts and Atlantic Storm-Track Experiment radio soundings. *Journal of Geophysical Research*, *108*.doi: 10.1029/2003JD003535.

Priestley, M. B. (1981). *Spectral analysis and time series*. *Academic Press*. London: Academic Press.

Prusa, B. J., Smolarkiewicz, P. K., and Wyszogrodzki, A. A. (1999). Parallel Computation of Gravity Wave Turbulence in the Earth ' s Atmosphere. *Society for Industrial and Applied Mathematics*, *32*(7), 1-5.

Prusaa, J. M., and Smolarkiewicz, P. K. (2003). An all-scale anelastic model for geophysical flows: dynamic grid deformation. *Journal of Computational Physics*, *190*(2), 601-622.

Prusa, J. M. and Gutowski, W. J. (2006). MULTI-SCALE WAVES IN SOUND-PROOF GLOBAL SIMULATIONS WITH EULAG. *Versita*, 1-23.

Ratna, S. B., Behera, S., Ratnam, J. V., Takahashi, K., and Yamagata, T. (2012). An index for tropical temperate troughs over southern Africa. *Climate Dynamics*. Doi: 10.1007/s00382-012-1540-8.

Richter, J., Chen, C., Garcia, R., Smith, A., and Bacmeister, J. (2010).Effects of gravity wave parameterization changes on the middle and upper atmosphere in the Whole Atmosphere Community Climate Model. *Geophysical Research Abstracts*, *12*, 3804.

Rossby, C. G. (1940). Planetary flow patterns in the atmosphere. *Planetary flow patterns*, 68-87.

Rossby, C. G., Namias, J., and Simmers, R. G. (1938). Fluid mechanics applied to the study of atmospheric circulations. *Papers in physical oceanography and meteorology*, *7*, 1-125.

Sato, K., Dunkerton, T. J., Miyahara, S., and Takahashi, M. (2009).he Roles of Equatorial Trapped Waves and Internal Inertia–Gravity Waves in Driving the Quasi-Biennial Oscillation. Part I: Zonal Mean Wave Forcing. *American Meteorological Society*, *67*(4).

Sheridan, S. C., and Lee, C. C. (2011).The self-organizing map in synoptic climatological research. *Progress in Physical Geography*, *35*, 109-119. doi: 10.1177/0309133310397582.

Shutts, G. J., and Vosper, S. B. (2011). Stratospheric gravity waves revealed in NWP model forecasts. *Quarterly Journal of the Royal Meteorological Society*, *137*(655), 303-317.

Smolarkiewicz, P. K., and Pudykiewicz, J. A. (1992).A Class of Semi-Lagrangian Approximations for Fluids. *Journal of the Atmospheric Sciences*, *49*(22).

Smolarkiewicz, P. K., and Margolinb, L. G. (1997). On Forward-in-Time Differencing for Fluids: an Eulerian/Semi-Lagrangian Non-Hydrostatic Model for Stratified Flows. *Atmosphere-Ocean*, *35*(1).

Song, I., Chun, H., Garcia, R. R., and Boville, B. A. (2006). Momentum Flux Spectrum of Convectively Forced Internal Gravity Waves and Its Application to Gravity Wave Drag Parameterization . Part II : Impacts in a GCM (WACCM). *Journal of the atmospheric Sciences*, *64*, 2286-2308.doi: 10.1175/JAS3954.1.

Todd, M. C., Washington, R., and Palmer, P. I. (2004). WATER VAPOUR TRANSPORT ASSOCIATED WITH TROPICAL – TEMPERATE TROUGH SYSTEMS OVER SOUTHERN AFRICA. *International Journal of Climatology*, *568*, 555-568. doi: 10.1002/joc.1023.

Tyson, P. D., and Preston-Whyte, R. A. (2002).*The Weather and Climate of Southern Africa*. Oxford University Press.

Vanneste, J. (2013). Balance and Spontaneous Wave Generation in Geophysical Flows. *Annual Review of Fluid Mechanics*, (September 2012), 147-172. doi: 10.1146/annurev-fluid-011212-140730.

Ventrice, M. J., and Thorncroft, C. D. (2012). A convectively coupled equatorial Kelvin wave ' s impact on African easterly wave activity * Corresponding Author Address : Michael J . Ventrice ,. *New York*. Albany.

Vosper, S. (2010).Stratospheric mountain waves generated by the southern Andes. In *14th Conference on Mountain Meteorology, Session 5, Mountain Waves and Rotors*.

Wallace, J. M., and Newell, R. E. (1966). Eddy fluxes and the biennial stratospheric oscillation. *Quarterly Journal of the Royal Meteorological Society*, *92*(394), 481-489.

Wang, L., and Geller, M. A. (2003). Morphology of gravity-wave energy as observed from 4 years (1998–2001) of high vertical resolution U.S. radiosonde data. *Journal of Geophysical Research Atmospheres*, *108*(D16).

Wang, L., Geller, M. A., and Alexander, M. J. (2005).Spatial and Temporal Variations of Gravity Wave Parameters. Part I: Intrinsic Frequency, Wavelength, and Vertical Propagation Direction. *Journal of the Atmospheric Sciences*, *62*, 125-142.

Wu, R., Kirtman, B. P., and Van Den Dool, H. (2010).ENSO Prediction Skill in the NCEP CFS.*US National Oceanic and Atmospheric Administration*.

Yuan, L., and Fritts, D. C. (1989). Influence of a mean shear on the dynamical instability of an inertia-gravity wave. *Journal of the Atmospheric Science*, *46*, 2562-2568.

Zagar, N., Tribbia, J., Anderson, J. L., and Raeder, K. (2009). Uncertainties of Estimates of Inertia – Gravity Energy in the Atmosphere . Part II : Large-Scale Equatorial Waves. *Monthly Weather Review*, *137*, 3858-3873. doi: 10.1175/2009MWR2816.1.

Zhang, S. D., Yi, F., Huang, C. M., and Zhou, Q. (2010). Latitudinal and seasonal variations of lower atmospheric inertial gravity wave energy revealed by US radiosonde data. *Annales Geophysicae*, *28*, 1065-1074. doi: 10.5194/angeo-28-1065-2010.

Zhang, Y., Xiong, J., Liu, L., and Wan, W. (2012). A global morphology of gravity wave activity in the stratosphere revealed by the 8-year SABER / TIMED data. *Journal of Geophysical Research*, *117*(February), 1-13. doi: 10.1029/2012JD017676.

Zwiers, F. W., and Storch, H. V. (2004).On the role of statistics in climate research. *International Journal of Climatology*, *24*(6), 665-680.